Volume 9
Number 38
14 October 2021
Pages 21465–22142

Journal of Materials Chemistry A

Materials for energy and sustainability

rsc.li/materials-a

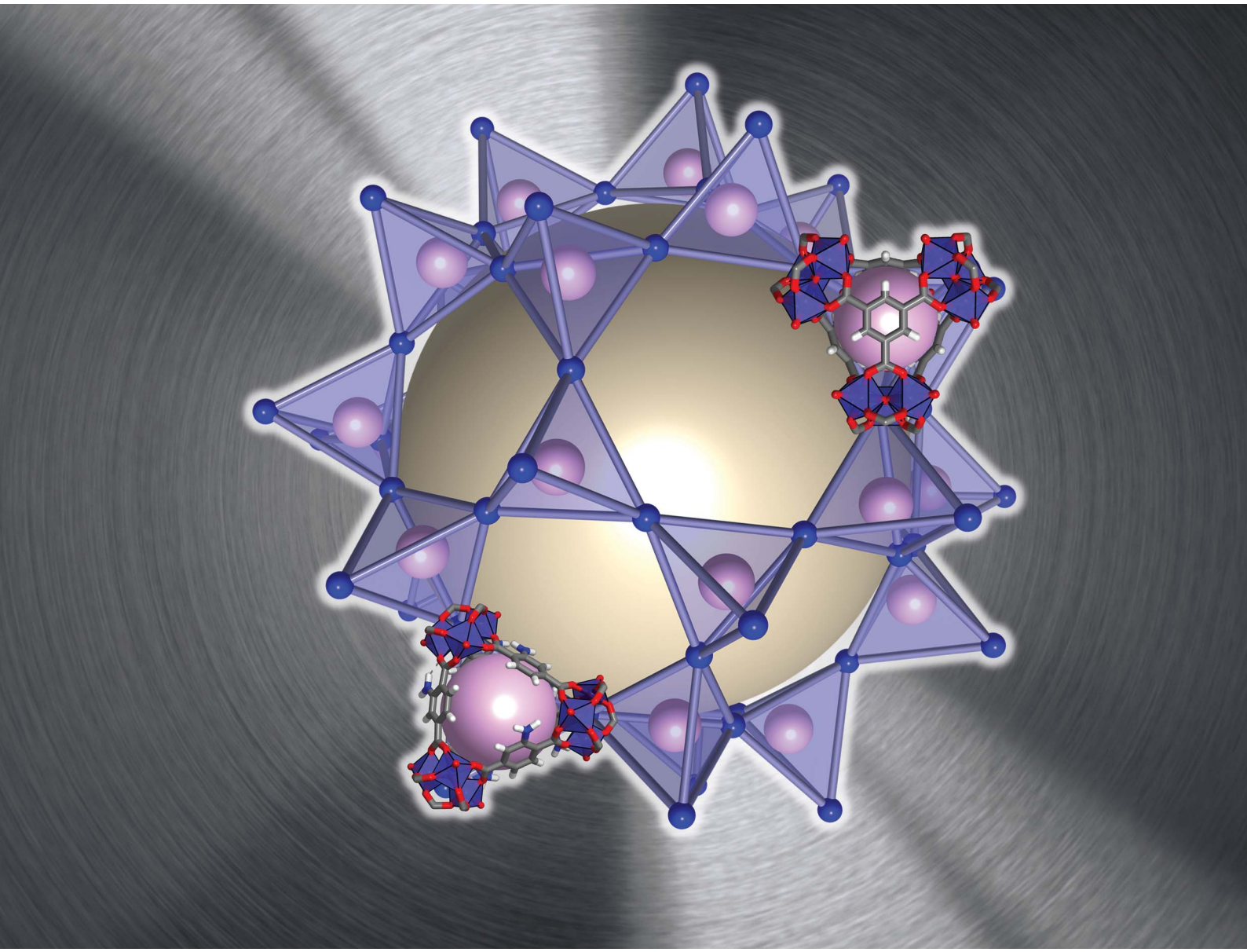

ISSN 2050-7488

ROYAL SOCIETY OF CHEMISTRY

REVIEW ARTICLE

Timothy Steenhaut, Yaroslav Filinchuk, Sophie Hermans
Aluminium-based MIL-100(Al) and MIL-101(Al) metal–organic frameworks, derivative materials and composites: synthesis, structure, properties and applications

Journal of Materials Chemistry A

ROYAL SOCIETY OF CHEMISTRY

REVIEW

Check for updates

Cite this: *J. Mater. Chem. A*, 2021, **9**, 21483

Aluminium-based MIL-100(Al) and MIL-101(Al) metal–organic frameworks, derivative materials and composites: synthesis, structure, properties and applications

Timothy Steenhaut, * Yaroslav Filinchuk* and Sophie Hermans *

Received 26th May 2021
Accepted 9th July 2021

DOI: 10.1039/d1ta04444c

rsc.li/materials-a

MIL-100(Al) and MIL-101(Al) are two related and particularly interesting mesoporous aluminium-based metal–organic frameworks (MOFs) that are able to adsorb and encapsulate a large panel of molecules and catalyse a wide range of reactions. Furthermore, they can be functionalized in many ways, or transformed into oxide or carbonaceous materials with interesting properties. In this review, we first cover various synthetic methods used for selectively obtaining these MOFs in a pristine state, including formation mechanisms and thermodynamic considerations. Then, the main applications of these materials, including catalysis, gas storage and adsorption of various chemical species, are addressed. Post-functionalization and encapsulation strategies to obtain MOF materials with improved properties are also discussed, as well as the advantages of such hybrid materials over the pristine MOFs. Furthermore, we describe synthetic methods for obtaining (doped) aluminium oxides and carbon materials from MIL-100(Al) and MIL-101(Al), together with their applications. By summarizing the main findings concerning those two particular MOFs and their derivatives, together with some pitfalls to avoid when characterizing them, we highlight unaddressed challenges and provide directions for future research.

1. Introduction to MIL-100(Al) and MIL-101(Al)

Metal–organic frameworks (MOFs) are porous coordination polymers that have great potential in many fields such as

Université Catholique de Louvain, MOST, Place Louis Pasteur 1, 1348 Louvain-la-Neuve, Belgium. E-mail: timothy.steenhaut@uclouvain.be; yaroslav.filinchuk@uclouvain.be; sophie.hermans@uclouvain.be

Timothy Steenhaut received his MSc Degree from the Université catholique de Louvain (Belgium) in 2017. His master thesis, run under the supervision of Prof. Sophie Hermans and Prof. Olivier Riant was awarded the Solvay prize of best Master thesis in 2017. He is currently a PhD candidate in the groups of Prof. Sophie Hermans and Prof. Yaroslav Filinchuk at UCLouvain. His work, funded by the FRIA doctoral grant of the F.R.S.-FNRS focusses on the development of greener synthesis pathways of stable and highly porous MOFs and their chemical modification for applications in gas sorption and catalysis.

Yaroslav Filinchuk studied Chemistry at Lviv National University and received PhD in Inorganic Chemistry in 2002. He joined the University of Geneva in 2000, where he begun to work on metal hydrides with Prof. Klaus Yvon. In 2006–2010 he worked at the Swiss-Norwegian Beam Lines at the European Synchrotron Radiation Facility. Since 2011 he is professor at the Université catholique de Louvain, Belgium. He received ESRF young scientist award in 2010 and published about 250 papers. His research interests include chemistry of hydrogen-rich solids, in particular for hydrogen storage, porous materials, and various applications of crystallography in materials science.

sorption of toxic molecules, ions[1–4] or greenhouse gases,[5–7] energy storage and conversion,[8–12] drug delivery,[13,14] sensing applications,[15,16] *etc.* Among the many possibilities of metal/ligands combinations, MOFs based on aluminium are particularly interesting because Al is the most abundant metallic element in the earth crust and its common oxidation state is +III,[17] which makes it a perfect candidate for the design of air-stable and robust MOF materials.[18] Furthermore, aluminium is a lightweight metal, making it particularly valuable for applications for which gravimetric considerations are important. Not surprisingly, several reviews dedicated to the general synthesis[18,19] and applications[20–22] of Al-based MOFs have already appeared. In this review, we will update those general aspects and more importantly focus on two important Al-based MOFs in particular, namely MIL-100(Al) and MIL-101(Al) to discuss them in greater detail. Those MOFs belong to the "MIL" family, which is a series of materials that was developed at the Lavoisier Institute in France, from which their names originate (MIL = Matériaux de l'Institut Lavoisier, or Materials of Lavoisier Institute).[23] Those materials are built from commercially available linkers, namely benzene-1,3,5-tricarboxylate (or trimesate, BTC^{3-}) for MIL-100(Al) and derivatives of terephthalate linkers for MIL-101(Al). Both materials possess the same topology and the same metal secondary building units (SBUs), thus giving them similar properties. The SBUs are carboxylate bridged trimeric μ_3-O centred aluminium clusters, having C_{3v} symmetry and the general formula $Al_3(\mu_3\text{-}O)(O_2CR)_6X_3$ (Fig. 1A). The aluminium atoms possess an octahedral geometry, the central oxygen atom linking the three metal centres of the SBU together, the four axial positions of each metal atom being occupied by μ_2-bridging carboxylates from the linkers and the apical positions (X) being occupied by solvent molecules and one anionic charge-balancing species per cluster to reach charge neutrality. The interconnection of four metal SBUs leads to the formation of supertetrahedra of which the aluminium clusters form the vertexes and the linkers form either the triangular faces, for MIL-100(Al), or the edges, for MIL-101(Al)

Sophie Hermans is an Inorganic Chemist who graduated from UCLouvain (Belgium). She started her research career as a synthetic chemist, making new clusters complexes. She obtained her PhD at the University of Cambridge (UK) under the supervision of Brian F. G. Johnson, then pursued postdoctoral studies with a Junior Research Fellowship in collaboration with Sir John M. Thomas. Back at UCLouvain, she started working on carbon-supported catalysts, synthesis and functionalization of nanostructured solids. She obtained the FNRS 'Chercheur Qualifié' and Assistant Professor positions in 2005 and was then promoted Full Professor in 2014 and FNRS 'Directrice de recherches' in 2020.

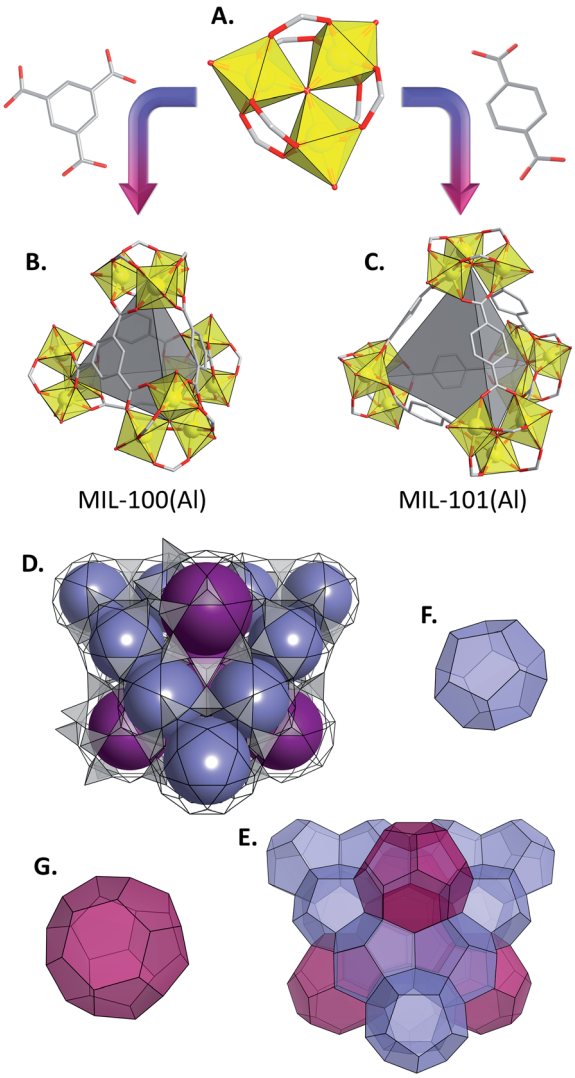

Fig. 1 Structure of (A) the $Al_3(\mu_3\text{-}O)X_3(O_2CR)_6$ clusters and the supertetraedra formed with (B) trimesate and (C) terephthalate linkers (color code: red = oxygen, grey = carbon, yellow = Al, hydrogens are omitted for clarity). The interconnection of supertetraedra (grey tetrahedra) (D) forms the framework of the MIL-100(Al) and MIL-101(Al) MOFs with large (purple) and small (blue violet) mesopores in the **mtn** topology (E). Details showing the pentagonal windows of the (F) small mesopores and pentagonal and hexagonal windows of the (G) large mesopores.

(Fig. 1B and C). The assembly of those microporous supertetrahedra leads to the formation of the framework, in the **mtn** topology (having the same framework as the material Zeolite Socony Mobil Thirthy-Nine, ZSM-39).[24] This type of framework is composed of two different interconnected mesoporous cages, which are 24 Å and 29 Å in diameter for MIL-100(Al), and 27 Å and 34 Å for MIL-101(Al) (Fig. 1D and E). The access to these mesoporous cavities is granted by microporous hexagonal and pentagonal windows (Fig. 1F and G).

MIL-100(Al) was first described by Volkringer *et al.* in 2009,[25] and is isostructural to its chromium and iron derivatives, which were discovered a few years earlier, in 2004 and 2007 respectively, by the same research group.[26,27] However, the assembly of

 This journal is © The Royal Society of Chemistry 2021

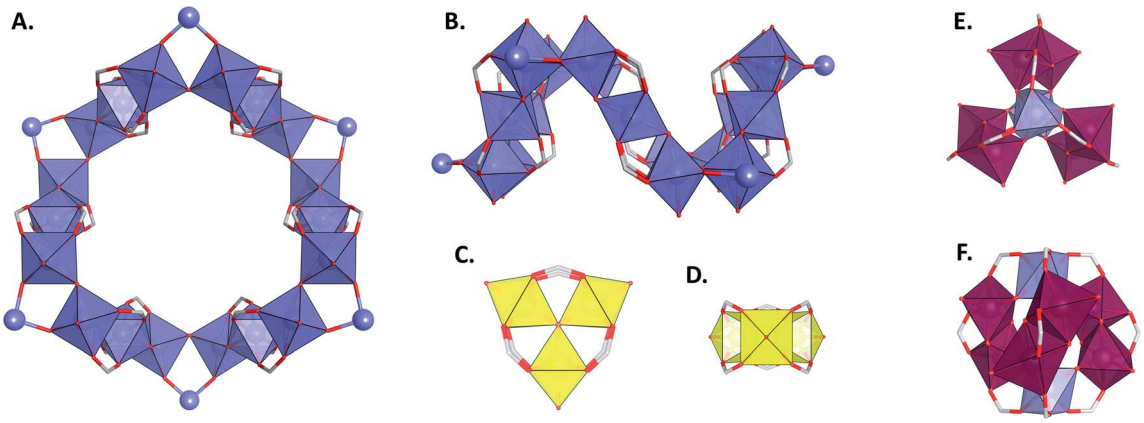

Fig. 2 Structures of the inorganic buildings units of MIL-96(Al), MIL-110(Al) and MIL-100(Al). (A and B) Hexagonal 18-membered rings formed from $AlO_2(OH)_4$ and $AlO_4(OH)_2$ of MIL-96. (C and D) $Al_3O(O_2CR)_6L_3$ units common to MIL-96(Al) and MIL-100(Al). (E and F) Aluminium octamers of MIL-110(Al). Aluminium atoms are represented as polyhedra of different colors depending on the connectivity (dark blue violet = chain-like, yellow = $Al_3(\mu_3\text{-}O)$; plum = edge-shared Al octahedra; light blue violet = corner-shared Al octahedra). Oxygen and carbon are represented in red and grey respectively, hydrogens are omitted for clarity.

aluminium centres with trimesate linkers can lead to the formation of several other types of MOFs, including, other than MIL-100(Al): MIL-96(Al) and MIL-110(Al). MIL-96(Al), discovered in 2006,[28] is similar to its gallium,[29] indium[30] and chromium[31] analogues and has the chemical formula $Al_{12}O(OH)_{18}(H_2O)_3(Al_2(OH)_4)BTC_6\cdot 24H_2O$. This microporous MOF possesses three types of cages built from the interconnection of two types of inorganic building units (Fig. 2A–D.). The first one consisting of a 2D network containing chains of $AlO_2(OH)_4$ and $AlO_4(OH)_2$ octahedra, which are interconnected to build hexagonal 18-membered rings (Fig. 2A and B). The second one is of the $Al_3O(O_2CR)_6L_3$ type (Fig. 2C and D), which is the same SBU as in MIL-100(Al), although this type of cluster is quite uncommon with aluminium and has not yet been encountered in any coordination complex before the discovery of MIL-96(Al). MIL-110(Al), having the chemical formula $Al_8(OH)_{12}\{(OH)_3(H_2O)_3\}BTC_3\cdot nH_2O$, was first described in 2007.[32] This MOF is composed of aluminium octamers (Fig. 2E and F) each connected to nine carboxylates from the trimesate linkers, which interconnect those units to form a three-dimensional structure possessing large hexagonal channels. It is worth mentioning that the structure of those three MOFs were solved by single crystal X-ray diffraction, the XRD data of MIL-110(Al) and MIL-100(Al) having been collected by microdiffraction setups which were revolutionary at the time of the discovery of those MOFs.

With terephthalic linkers, MOFs other than those of the MIL-101(Al) type are MIL-53(Al), MIL-68(Al) and MOF-235(Al). MIL-53(Al), which was discovered in 2004,[33] is similar to its chromium and iron counterparts. It possesses one-dimensional channels with structural flexibility and breathing behaviour upon introduction of guest molecules (Fig. 3A and B) and exists with a plethora of substituted linkers.[34–40] The high thermal stability of this framework (decomposition above 500 °C), as well as the fact that it can be synthesized by green methodologies has led to its industrial production by BASF under the name

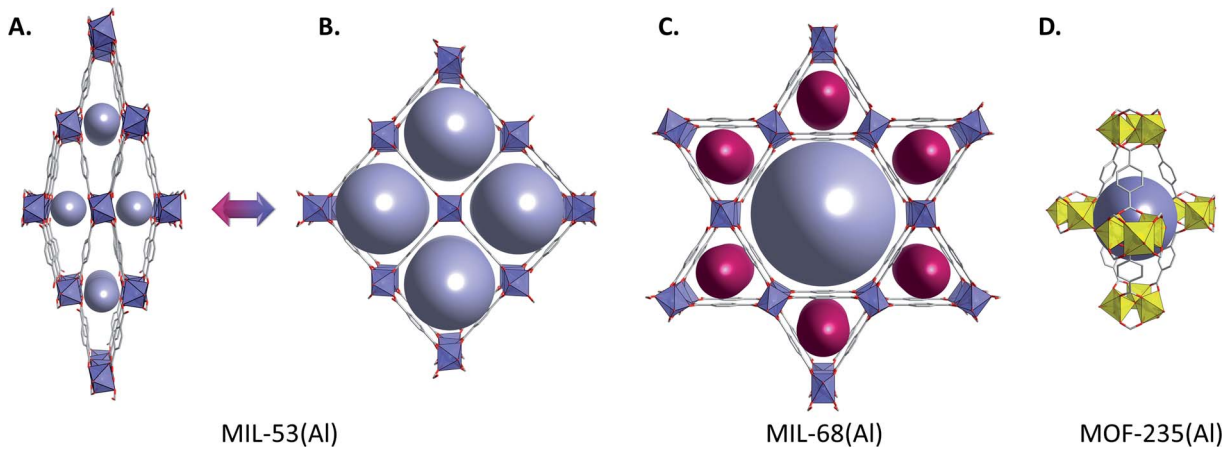

Fig. 3 Structure of (A and B) MIL-53(Al), (C) MIL-68(Al) and (D) MOF-235(Al) (color code: red = oxygen, grey = carbon, blue violet = Al chains, yellow = Al clusters, hydrogens are omitted for clarity).

Basolite® A100,[41] being one of the first MOFs produced on a large scale and commercialized. For more information about this MOF, the reader is referred to specialized reviews.[42] MIL-68(Al) is a rigid framework which has a structure similar to its chromium and iron analogues,[43] and possesses two type of porous channels (Fig. 3C). MOF-235(Al) has a similar structure to MOF-235(Fe) (Fig. 3D) and is a metastable phase, as we will discuss below.[44–46] As for chromium and iron, the existence of all those framework topologies built from a unique metal and type of linker is responsible for the need of well-defined synthesis strategies, which are crucial in the determination of the obtained material.

2. MIL-100(Al)

2.1 Synthesis and thermodynamic stability

MIL-100(Al) was first obtained as a highly porous ($S_{BET} = 2152$ m^2 g^{-1}) yellow powder, with thermal stability up to 370 °C (in oxidizing atmosphere), by hydrothermal reaction of $Al(NO_3)_3 \cdot 9H_2O$, HNO_3 and trimethyl-1,3,5-trimesate as linker source at 210 °C for 3 to 4 h.[25] Tedious control of the pH was crucial for this synthesis as it had to be set precisely at values between 0.5 and 0.7, lower pH values leading to the formation of MIL-110(Al) and longer reaction times yielding MIL-96(Al). On the contrary to MIL-100(Cr) and MIL-100(Fe), which could only be obtained as crystalline powders, very small single crystals of this MOF could be obtained and the structure was solved by micro-diffraction using synchrotron radiation (ID13 beamline at ESRF, Grenoble, France), leading to the first structural characterization of a MIL-100 MOF by this technique. Furthermore, the MOF was also characterized by means of solid-state ^1H, ^{13}C and ^{27}Al NMR, which was fully consistent with the XRD structure. *In situ* NMR and *ex situ* XRD and SEM studies were performed in another work to get insight into the reaction mechanism responsible for the MOF's formation (Fig. 4).[47] In this study, the synthesis parameters were slightly modified to be able to perform the reaction in a Teflon-lined Vespel tube. The reaction was run at 180 °C, allowing slower kinetics, and thus facilitating the follow-up of the reaction progress. The obtained results pointed out that MIL-100(Al) is the kinetic product, whereas MIL-96(Al) is the thermodynamic one. ^{27}Al solution-state NMR showed that at least four different Al-based species are formed during the reaction, $Al(H_2O)_6^{3+}$ being the main species present (Fig. 4, inset). When heating of the mixture is started, a 1 : 1 Al-BTC complex forms, leading to partial solubilisation of the linker. In later stages, dimeric species giving distinct ^{27}Al NMR signals are formed; first Al_2-BTC_1, having one BTC unit bridging both metal centres, and then Al_2-BTC_2, containing two BTC units. The formation of those two species has been explained by the slow solubilisation of BTC by decomposition of trimethyl-1,3,5-benzenetricarboxylate over the course of the reaction. The last dimeric unit, Al_2-BTC_2, is contained in both MIL-100(Al) and MIL-96(Al) structures. The Al_2-BTC_1 species was stabilized under more acidic conditions, explaining that MIL-110(Al), which contains this unit in its structure, is the only crystalline phase that is formed at extremely low pH. The study did not evidence any trimeric $Al_3(\mu_3\text{-}O)$ species in solution. The kinetic nature of MIL-100(Al) and the thermodynamic one of MIL-96(Al) was corroborated by other studies,[48–50] and it was shown that fast heating methods, such as microwave irradiation, enable isolation of thermodynamically unstable MOFs such as MIL-100(Al) more easily and much more rapidly than through conventional heating. However, all these synthetic procedures need tedious control of the reaction parameters as MIL-96(Al) and/or MIL-110(Al) often form if small changes are applied to the procedure. Moreover, it has recently been shown that adding some acetic acid in the reaction mixture allows the formation of missing cluster defects into the MOF, as evidenced by TGA.[51]

Alternative synthesis procedures have been developed since then (Table 1), some of which having only small differences with the initial one. For example, the reaction mixture can be slowly ramped to 210 °C at 3 K min^{-1} and the heating maintained for three days instead of 3–4 h, followed by extraction with hot ethanol for 16 h, yielding a yellow powder with a PXRD pattern corresponding to MIL-100(Al).[52] Although this procedure allows obtaining a material with no extra-framework trimesic acid, a small amount of $Al(OH)_3$ was detected in the obtained solid by ^{27}Al, ^1H and heteronuclear correlation solid-state NMR spectroscopy.[53] This probably explains the much lower BET surface area (1482 m^2 g^{-1}) of the obtained material.

Trimesic acid can also be used instead of trimethyl-1,3,5-trimesate as cheaper source of linker. One way to achieve this is by generating the ester *in situ* during the synthesis by addition of methyl or ethyl containing molecules, typically methanol, ethanol, *N*,*N*-dimethylformamide (DMF) or *N*,*N*-diethylformamide (DEF), into an aqueous reaction mixture composed of aluminium nitrate, HNO_3 and H_3BTC.[54]

Heating this mixture at 200 °C leads to the formation of MIL-100(Al) with BET surface areas up to 1920 m^2 g^{-1} over a 4 h period of time. Control of pH (ideally at pH = 1.6 when DMF is used), as well as controlling the nature and stoichiometry of the used methyl or ethyl containing molecules is crucial for the outcomes of the synthesis. Using alkaline methylamine or dimethylamine, as well as using $-CH_3$/–COOH or $-C_2H_5$/–COOH ratios higher than 1 leads to the formation of MIL-96(Al) as by-product.

The use of cetyltrimethylammonium bromide (CTAB) as surfactant in the synthesis of aluminium trimesate MOFs has also been studied at lower synthesis temperatures (120 °C) in water/ethanol mixtures by using trimesic acid as linker source.[55] In this case, MIL-100(Al) with a BET surface area of 1550 m^2 g^{-1} could be selectively obtained when the H_2O/EtOH ratio was kept below 1.5 at pH 2.5. Higher concentrations of water in the medium led to the formation of MIL-96(Al) as secondary phase and lower pH values to MIL-110(Al). Through the use of CTAB as surfactant, MIL-100(Al) was obtained as agglomerates of small MOF nanoparticles, leading to the formation of inter-particle mesoporous voids, giving a material with hierarchized porosity. Similar hierarchized porosity can also be obtained without surfactant by solvothermal heating at mild temperatures (80 °C) of aluminium chloride and trimesic acid in mixture of ethanol, DMF and water, with HCl as modulator.[60]

 This journal is © The Royal Society of Chemistry 2021

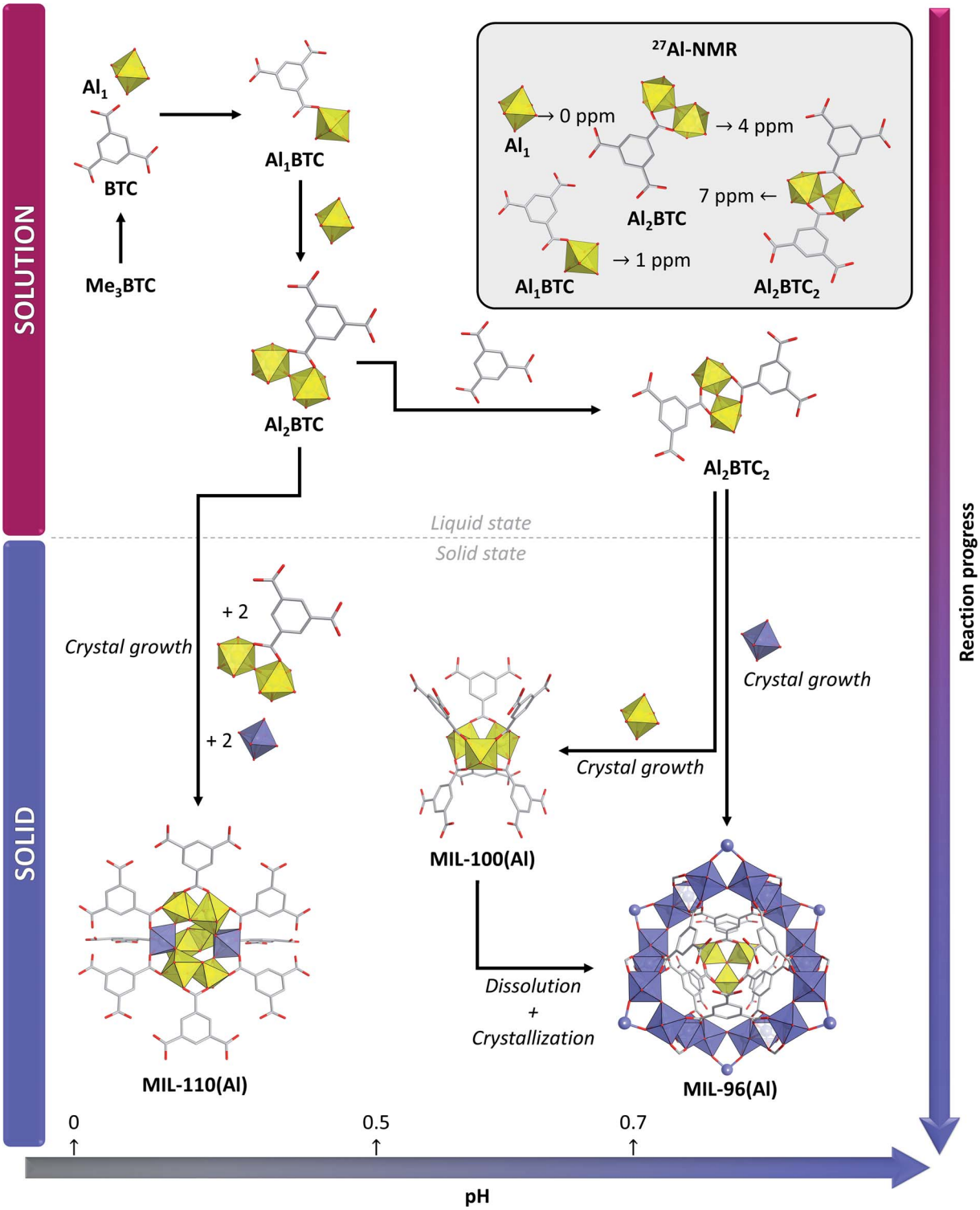

Fig. 4 Formation mechanism of MIL-110(Al), MIL-96(Al) and MIL-100(Al) under hydrothermal conditions from trimethyl-1,3,5-trimesate and aluminium nitrate, as deduced from *in situ* solution state NMR and *ex situ* diffraction experiments. The inset indicates the ^{27}Al-NMR chemical shifts for of the different species observed in solution. Colour code: yellow and blue = different types of Al clusters, grey = C, red = O. Hydrogen are omitted for clarity. Adapted from ref. 47.

It has also been reported that MIL-100(Al) could be selectively obtained through microwave irradiation of an aqueous suspension of aluminium nitrate and trimesic acid in the presence of an inducing agent.[56] Different inducing agents were tested and it was shown that aluminophosphate molecular sieves, SAPO-11 and SAPO-34, as well as Al-, Ni- and Co-based

Table 1 Different synthesis pathways to obtain MIL-100(Al), reaction conditions and BET surface areas of the obtained MOFs (for activation procedures, the reader is referred to the corresponding references)

S_{BET} ($m^2\ g^{-1}$)	Notes	Reactants and conditions	Ref.
2152		$Al(NO_3)_3 \cdot 9H_2O$, HNO_3, Me_3BTC, water, 210 °C, 3 to 4 h	25
1056	*	$Al(NO_3)_3 \cdot 9H_2O$, H_3BTC, water, MW (210 °C), 1 min	48
1701		$Al(NO_3)_3 \cdot 9H_2O$, HNO_3, Me_3BTC, water, MW (200 °C, 1200 W), 83 min	49
300	†	$Al(NO_3)_3 \cdot 9H_2O$, HNO_3, H_3BTC, water, MW (210 °C), 30 min	50
2400	†	$Al(NO_3)_3 \cdot 9H_2O$, HNO_3, Me_3BTC, water, MW (210 °C), 30 min	50
1482	‡	$Al(NO_3)_3 \cdot 9H_2O$, HNO_3, Me_3BTC, water, 210 °C, 3 days	52
1920		$Al(NO_3)_3 \cdot 9H_2O$, HNO_3, H_3BTC, water, DMF (210 °C), 4 h	54
1550–1970		$Al(NO_3)_3 \cdot 9H_2O$, H_3BTC, water, cetyltrimethylammonium bromide, EtOH, 120 °C, 12 h	55
1534–1576	⁂	$Al(NO_3)_3 \cdot 9H_2O$, H_3BTC, water, inducing agent (insoluble phosphate), MW (190 °C, 300 W), 10 min	56
1761–1795	⁂	$Al(NO_3)_3 \cdot 9H_2O$, H_3BTC, ethanol, 120 °C, 1 h	57
920	⁂	$Al(NO_3)_3 \cdot 9H_2O$, H_3BTC, ethanol, 120 °C, 1 h	58
1670		$Al(NO_3)_3 \cdot 9H_2O$, H_3BTC, water, MW (1200 W), 5 min	59

phosphates were efficient for selective synthesis of MIL-100(Al), whereas molecular sieves that do not contain phosphate moieties (*i.e.* ZSM-5, MCM-41 or SBA-15) were not able to play this role. In the absence of any inducing agents, MIL-96(Al) was formed as single phase. The synthesis mechanism was investigated and it was shown that the gradual release of phosphate groups from the surface of the inducing agent was necessary for the selective nucleation of MIL-100(Al). In the absence of phosphate in the inducing agent, or by using freely soluble phosphates (Na_3PO_4, Na_2HPO_4, NaH_2PO_4), pure MIL-100(Al) could not be obtained. SEM analysis showed that the formation of MIL-100(Al) occurred at the surface of the inducing agent, which was consumed (dissolved) during the synthesis.

MIL-100(Al) can also be obtained in the form of a gel through reaction of $Al(NO_3)_3 \cdot 9H_2O$ with trimesic acid in an ethanol solution at 120 °C.[57] The obtained gel can then be transformed into an aerogel by drying under air, or into a xerogel by using a supercritical CO_2 drying process. Although the obtained gels are not crystalline, they possess high BET surface areas of 1761 $m^2\ g^{-1}$ and 1795 $m^2\ g^{-1}$ for the xero- and aerogel, respectively. Another study exploited the same synthesis strategy to obtain MIL-100(Al) aerogels with a BET surface area of 920 $m^2\ g^{-1}$.

Electrochemical synthesis of MIL-100(Al) has also been attempted by anodic dissolution.[61] However, no crystalline product could be obtained when this procedure was applied for this MOF, on the contrary to the copper-based MOF HKUST-1 used as model in the same study, for which nucleation takes place almost instantly. The slower nucleation rate of MIL-100(Al) might explain the failure of this synthetic approach.

2.2 Activation and open-metal sites

^1H MAS and $^{13}C\{^1H\}$ CPMAS spectra of MIL-100(Al) obtained through the initial synthesis procedure of Volkringer *et al.* evidenced that the as-synthesized MOF contains trapped extra-lattice trimesic acid molecules.[25] These could be removed by solvothermal activation in DMF at 150 °C for 4 h, followed by refluxing in water for 12 h, yielding a sample with a BET surface area of 2152 $m^2\ g^{-1}$ after degassing overnight at 220 °C. This activation process was further monitored by tedious solid-state NMR experiments and elemental analysis in another study.[62] The results showed that upon activation, there was a slight excess of N and C contents compared to the theoretical values expected for a fully activated MOF, indicating that a small fraction of H_3BTC, nitric acid and DMF remains in the pores of the MOF. Nevertheless, most of the guest molecules were removed during the solvothermal activation process and were replaced by water, in a fixed ratio of $15H_2O/1H_3BTC$. The formulae of the as-synthesized and activated MOFs were determined to be $Al_3O(OH)(BTC)_2(H_2O)_{16}(H_3BTC)_{0.9}(HNO_3)_{1.3}$ and $Al_3O(OH)(BTC)_2(H_2O)_{22-25}(H_3BTC)_{0.3}(HNO_3)_{0.2}$ respectively. Quantitative ^1H and ^{27}Al NMR experiments showed that only one out of three aluminium atoms per trimer could be coordinatively unsaturated after thermal activation at 250 °C (Fig. 5A), leading to a pentacoordinated Al center, contrary to MIL-100(Cr), in which two metal centres can be decoordinated (Fig. 5B). Heating at higher temperatures does not allow removal of any supplementary water molecules. ^{27}Al–^{13}C proximities in MIL-100(Al) were further probed by dynamic nuclear polarization enhanced NMR spectroscopy.[63] These 2D experiments allowed assigning the ^{13}C resonances, further validating the crystal structure of the MOF. In another study, NMR experiments on an activated sample revealed that about 50% of the Al sites of the material were five coordinated. In this case, the excess of five-coordinated sites might be explained by the presence of $Al(OH)_3$ resulting from a different synthetic procedure.[53]

The open-metal sites generated after thermal activation in MIL-100(Al) leads to the presence of Lewis acidic sites, as shown by IR spectroscopy of various probe molecules adsorbed into the activated MOF, including CO, pyridine and CD_3CN.[64] Quantitative measurements with CO and pyridine confirmed the fact that only one out of three Al sites can be activated, whereas pyridine and CD_3CN adsorption experiments revealed strong acidity, similar to that of silica-alumina, which can be expected as no trivalent cation has a higher polarizing power than Al^{3+}. However, CO experiments revealed a weaker acidity. This last

 This journal is © The Royal Society of Chemistry 2021

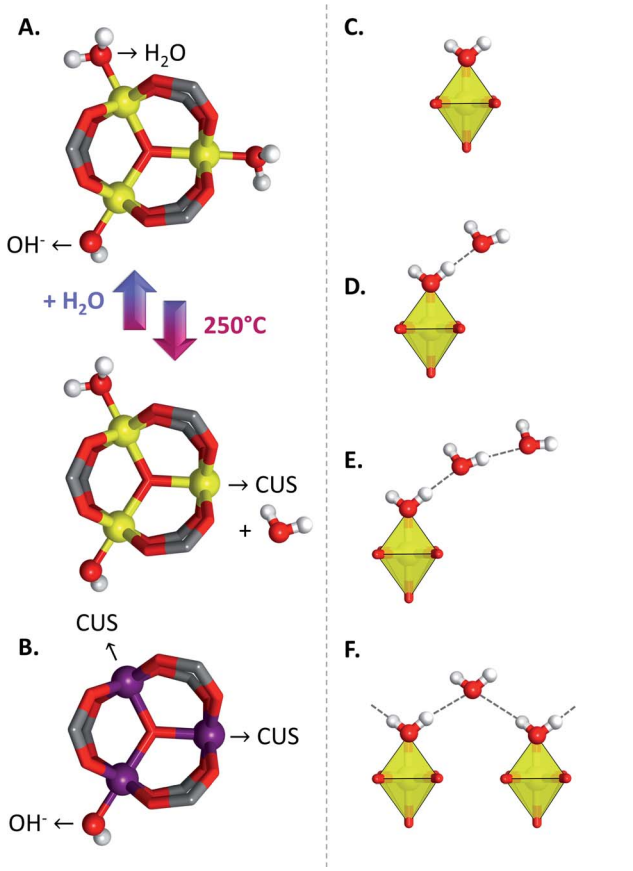

Fig. 5 (Left) (A) Thermal activation of MIL-100(Al) evidencing the formation of one coordinatively unsaturated site (CUS) and activated form of (B) MIL-100(Cr) having two CUSs. (Right) Origin of Brønsted acidity of water coordinated to the aluminium of MIL-100(Al) through the polarization of water by the formation of (C) a monomer, (D) a dimer, (E) a multimer and (F) water molecules linked by hydrogen bonding to two other water molecules each polarized by two different Al atoms.

observation evidences the usefulness of using a variety of probes for proper determination of the acidity of MOFs, in order to avoid drawing hasty conclusion from the results of isolated experiments. Indeed, in this case the use of CO as probe molecule, because of its lower basicity than the other probes, led to an underestimation of the acidity of the material, although this technique enabled proper quantification of the amount of CUSs, in agreement with NMR data of previous reports. Brønsted acidity was also evidenced and was attributed to water molecules within the coordination sphere of Al. Those water molecules can give rise to different acidic species, such as simply coordinated water (monomer) (Fig. 5C), water molecules that are H-bonded to one coordinated water molecule in the form of dimers (Fig. 5D) or multimers (Fig. 5E), or hydrogen-bonded water molecules coordinated to two coordinated H_2O molecules (Fig. 5F). Interestingly, when MIL-100(Al) is fully hydrated, only this last species is responsible for the Brønsted acidity of the material. Adsorption of bromothymol blue as acidity indicator dye on MIL-100(Al) showed however that this acidity is moderate compared to some benchmark Brønsted acidic solids, such as ZSM-5 or $H_3PMo_{12}O_{40}$.[60] The interaction and motional behaviour of pyridine-D_5 within MIL-100(Al) has also been studied more recently through ^2H solid-state NMR, evidencing bound states to the coordinatively unsaturated sites (CUSs) and Al–OH sites, as well as mobile states. Above 333 K, the mobile states are mainly populated, whereas at lower temperatures both coordinated and mobile states are occupied.[65]

2.3 Lewis acid catalysis

The metal centres of pristine MIL-100(Al) and MIL-101(Al) are in the stable +III oxidation state and are therefore not able to perform redox reactions[66,67] or to stabilize oxidation sensitive species such as Cu(I), in contrast to MIL-100(Fe).[68] However, the Lewis acidity of the Al(μ_3-O) SBUs enables the use of MIL-100(Al) as acid catalyst in a variety of reactions. The acidity of MIL-100(Al), MIL-96(Al) and MIL-110(Al) was probed by a spin probe method using EPR spectroscopy with the 2,2′,6,6′-tetramethyl-1-piperidinyoxyl (TEMPO) radical as probe molecule, as well as by IR spectroscopy employing benzonitrile as acidity probe.[69] Both methods allowed to determine that the amounts of Lewis acidic sites in the MOFs decreased in the order MIL-100(Al) > MIL-110(Al) > MIL-96(Al). Those MOFs were investigated for their ability to catalytically rearrange α-pinene oxide to campholenic aldehyde (CA) in dichloroethane at 30 °C and it was shown that the activity and selectivity towards CA followed the same sequence as the Lewis acidity of the MOFs. The good selectivity of MIL-100 for CA was explained by shape selectivity due to the size of the pores and windows within the MOF. Further comparison of the catalytic properties was performed with the Fe and Cr analogues of MIL-100(Al) and revealed that the selectivity towards CA decreased according to: MIL-100(Al) > MIL-100(Fe) > MIL-100(Cr), in agreement with the electronegativity of the metal centres. It was also shown that MIL-100(Al) was more efficient than MIL-110(Al) and MIL-96(Al) for catalysing the formation of 1,5-benzodiazepine from the reaction of 1,2-phenylenediamine with acetone, according to its more significant acidity.[70] However, the yield of benzodiazepine obtained with MIL-100(Al) as catalyst was lower than the one obtained when using its Cr, Fe and V derivatives, as those metals possess a lower ionic potential, resulting in higher complexing strength to amine groups. In a recent study, MIL-100(Al) and MIL-96(Al) were compared for the catalytic conversion of *p*-chlorobenzaldehyde into acetals by reaction with various alcohols.[71] It was shown that MIL-100(Al) was much more efficient for performing this reaction than was MIL-96(Al). The reaction proceeded well with small alcohols such as methanol and ethanol, whereas the larger alcohols, 1-propanol and 1-butanol, showed nearly no conversion. It was observed that the unactivated form of MIL-100(Al) was more efficient for the catalytic reaction than its activated form, due to the Brønsted acidity of the water molecules. However, the recyclability of the materials after reaction was not evaluated to determine whether the initial activity is maintained upon contact with the reactants and products of the reaction. Furthermore, through the use of solid-state ^{27}Al NMR and

crystallographic investigations, this study evidenced an important role of the size of the pore windows and catalytic pockets for the diffusion of reactants and products and efficiency of the catalytic reaction, explaining the low conversions observed for 1-propanol and 1-butanol. MIL-100(Al), as well as several other Al-based MOFs such as DUT-4, DUT-5, MIL-53 and NH_2-MIL-53, were found active for the sulfoxidation reaction of thioanisole to methyl phenyl sulfoxide by reaction with 35% H_2O_2.[49] Pristine MIL-100(Al) was also shown to be efficient in the Knoevenagel condensation reaction of benzaldehyde with malononitrile, for which it showed better activity than the Cu-MOF HKUST-1 and the Zr-MOF UiO-66.[72] IR spectroscopy with $CDCl_3$ as probe molecule allowed to determine that the MOF contains basic sites, which likely arise from the formation of "M^{n+}–O^{2-} Lewis acid–base" pairs between the metal centre and oxygenated ligands of the MOF (μ_3-O^{2-} and carboxylates). Those enable the reaction to proceed, which is also facilitated by the acidic sites on which the aldehyde can coordinate. Very recently, it has been evidenced that advantage can be taken of the strong interactions of the Al 3p orbitals of the metal centres in MIL-100(Al) with the N 2p orbitals of N_2 to use this MOF as electrocatalyst for the synthesis of ammonia in KOH solution.[51] The strong binding of nitrogen to the aluminium in the MOF allows gradual binding of H^+ to the nitrogen, cleaving the N≡N triple bond and reducing N_2 to hydrazine (NH_2NH_2) and then to ammonia, while the use of KOH allows to suppress the competing hydrogen evolution reaction. However, it should be mentioned that the authors of this study did not perform XRD measurements to assess whether the MOF's crystalline structure was stable under the conditions used for catalysis. The observed activity could thus be due to degradation products originating from the reaction of MIL-100(Al) with the alkaline reaction medium, instead of to the MOF itself.

2.4 Gas sorption and separation

Although MOFs can be used as adsorbents in both solution and gas phase, surprisingly little attention has been paid to the latter for pristine MIL-100(Al). Indeed, it seems that gas phase absorption in MIL-100(Al) has only been studied experimentally for NO at low pressure onto the Lewis acid sites of MOF, methane, hydrogen at 4 MPa for MIL-100(Al) and Pd@MIL-100(Al) (see MIL-100(Al) composites below), and methyl iodide. These will be discussed below. Regarding solution phase adsorption studies, it will be covered in the next section.

Several studies were dedicated to the adsorption of the paramagnetic biological signalling but toxic nitric oxide (NO) gas. First, low-temperature studies by IR measurements showed that NO interacts weaker with MIL-100(Al) than with MIL-100(Fe).[52] However, the presence of EPR silent Al^{3+} centres allowed following the temperature-dependent NO adsorption by EPR spectroscopy in complement to the FTIR measurements. This encouraged further investigation, in which complementary low temperature high-resolution pulse EPR methods and DFT calculations allowed to distinguish three different binding sites for NO in the framework.[73] The first binding site could be attributed to the open-metal site of the MOF, whereas the exact nature of the two other sites could not be determined, but one of those is likely due to interaction of NO with the organic part of the MOF and might be a general situation for all types of MOFs. Independently, solid-state NMR experiments showed that NO also interacts with the CUSs of MIL-100(Al) at room temperature.[53] This was evidenced by a decrease of the signal corresponding to five-coordinated aluminium in favour of six-coordinated species in the ^{27}Al spectra of the activated sample in the presence of NO. Furthermore, FTIR spectra revealed the presence of NO^+ species under these conditions.

Regarding the adsorption of methane by MIL-100(Al), only one measurement has been reported in the literature.[54] Nevertheless, the obtained gravimetric storage capacity of the MOF, namely 3.05 mmol g^{-1} at 25 °C, outperforms the ones reported for MIL-100(M) MOFs based on other metals (M = Cr, Fe and V). This interesting feature can easily be explained by the much lighter weight of the metal centers.

Concerning methyl iodide, breakthrough experiments were performed with a mixture of MeI diluted in argon on a fixed bed of the activated MOF.[74] However, MIL-100(Al) did not show any specific affinity for methyl iodide and performed quite badly in the tests, on the contrary to other MOFs with smaller pore windows having a size similar to MeI.

The interaction of CO_2 gas in MIL-100(Al) and isostructural Sc, Cr and Fe MOFs was first studied by *ab initio* modelling.[75] However, this study does not give any experimental values for MIL-100(Al) for comparison. In a recent experimental study, we showed that MIL-100(Al) in fact possesses a unique adsorption behaviour that distinguishes it from its isostructural counterparts composed of other metals based on Fe and Cr. Indeed, volumetric sorption isotherms of CO_2 at room temperature revealed a non-classical uptake that does not follow a typical Langmuir isotherm once the pressure exceeds 25 bar, pressure at which a slowing down of the sorption kinetics and an increase of the excess uptake is observed. This particular behaviour is thought to be due to the presence of the coordinated water molecule on the Al_3-(μ_3-O) clusters, and the formation of a carbonic acid species at high pressures.[60]

2.5 Adsorption of liquids and dissolved species

Water adsorption in MIL-100(Al) is of particular interest as it could lead to the development of various practical applications. One of those is directly based on the heat exchange processes that occurs during adsorption and desorption of water in the MOF.[76] Indeed, during evaporation, water takes up evaporation heat (Q_{evap}) and when the evaporated water is taken up in the MOF by adsorption, heat (Q_{ads}) is generated. For desorbing the water of the MOF, heat must be applied (Q_{des}) and the desorbed water then condenses, releasing condensation heat (Q_{cond}). Advantage can be taken from those enthalpies for constructing MOF-based sorption chillers or heat pumps. It has been demonstrated that MIL-100(Al), as well as its iron counterpart, presents water sorption isotherms with suitable features for such applications, like a small hysteresis and high uptakes. Furthermore, the MOF shows good stability, with only negligible decomposition and surface area loss (~5.9% loss in BET

 This journal is © The Royal Society of Chemistry 2021

surface area) upon 40 adsorption/desorption cycles. Interestingly, the crystallinity of MIL-100(Al) seems to improve upon several cycles, as indicated by narrowing of PXRD peaks. Another study reported that MIL-100(Al) and MIL-96(Al) both demonstrate high stability in a 75% RH atmosphere upon 40 cycles between 40 and 140 °C, whereas MIL-110(Al) degraded under these conditions as shown by PXRD measurements.[77] Furthermore, this study concluded that MIL-100(Al) was the only aluminium trimesate MOF that could be regarded as a potential candidate for water sorption applications. Indeed, its water sorption capacities (0.7 g H_2O per gram of material under the tested conditions) are outperforming those of the two other MOFs, as well as the one of ZnBTC MOF. MIL-100(Al) has also been studied for production of fresh water from moist air.[78] It has been shown that the working capacities (*i.e.* the difference in the adsorbed amount under adsorption and desorption conditions) of this MOF outperform the ones of its iron and chromium counterparts in cases were the relative humidity fluctuates between 0.05 and 0.35 (working capacity of 358 $cm^3\ g^{-1}$) as well as between 0.30 and 0.55 (405 $cm^3\ g^{-1}$). Only in conditions were $0.00 \leq P/P_0 \leq 0.45$ (526 $cm^3\ g^{-1}$), MIL-100(Fe) performs better (747 $cm^3\ g^{-1}$) and even only during the first adsorption cycle. Furthermore, the working capacity of MIL-100(Al) remains stable after 5 cycles, and the crystallinity of the MOF is preserved, making MIL-100(Al) a good candidate for water harvesting. The diffusion mechanisms of water through beds of MIL-100(Al) has also been studied through a combination of computed molecular dynamics and pulsed field gradient (PFG) NMR.[79] Those methods provided a theoretical model, which corroborated the observations made in the experimental studies of water adsorption cited above. Furthermore, PFG NMR evidenced that there is an exchange of H_2O molecules between the inter- and intracrystalline space.[80] The results show that the intracrystalline mean residence time of the water molecules decreases with increasing temperature, allowing determination of the activation energy of the exchange by PFG NMR.

Although the adsorption of organoarsenic compounds is much lower for MIL-100(Al) than for MIL-100(Fe),[81] the removal of toxic inorganic arsenate by MIL-100(Al) and MIL-100(Fe) has been studied by adsorption experiments using aqueous solutions containing $HAsO_4^{2-}$ ions.[82] The adsorption capacity of both MOFs was similar, MIL-100(Al) (128 mg g^{-1}) being slightly more efficient than its iron counterpart (124 mg g^{-1}). Those values were compared to the ones reported for other porous materials and Fe- and Al-based nanomaterials, demonstrating that the MIL-100 MOFs were far more efficient for this application. FTIR measurements revealed the presence of Fe–O–As(v) and Al–O–As(v) bands, showing that the adsorption occurred at the CUSs. Interestingly, the long-range order of the MOFs was disturbed upon adsorption of arsenates, leading to disappearance of some of the X-ray diffraction peaks. The crystallinity of the materials could be recovered by desorption of the arsenate ions under acidic conditions. The same study showed that the same long-range disruption occurred when large organic molecules such as methylene blue, Coomassie Brilliant Blue G-250 and rhodamine B (RhB) were adsorbed by MIL-100(Fe) and MIL-100(Al). Furthermore, it was demonstrated that those MOFs were efficient in the removal of such organic dyes from water, the removal of RhB by MIL-100(Al) however being less efficient. The capture of actinides (Th^{4+} and $[UO_2]^{2+}$) as well as a lanthanide ion (Nd^{3+}) from aqueous solutions by activated MIL-100(Al) has also been studied.[83] The cations were adsorbed in about 15 minutes, and the adsorption efficiency was dependent on the Lewis acidity of the adsorbate, *i.e.* Th^{4+} (95% removal) > $[UO_2]^{2+}$ (79%) > Nd^{3+} (73%), in accordance with the experimentally determined enthalpies of the process. A thermal treatment after absorption allowed the formation of oxide nanoparticles within the pores of the MOF, allowing definitive encapsulation of the actinides or neodymium. MIL-100(Al) could thus be used as adsorbent for radionuclides in the event of a nuclear accident. MIL-100(Al) also shows efficient and selective removal of several N-heterocyclic molecules over nitrobenzene, 2-bromoaniline and thiophene in *n*-heptane.[56] The highest removal efficiency was demonstrated for pyridine (1.38 mmol g^{-1}), followed by quinoline (1.09 mmol g^{-1}). Steric effects of the substituents explained lower adsorptions of 2-methylpyridine and 2-dichloropyridine.

2.6 Encapsulation of chemical species

Thanks to its porous nature and good stability, MIL-100(Al) can be used as template for encapsulation of various chemical species. This can be done for catalytic applications, by incorporation of catalytically active metal complexes for example. Tris(1,10-phenanthroline) Cu(II) complexes (Fig. 6A) were incorporated in MIL-100(Al) by impregnation of $CuCl_2$ in a an aqueous solution, followed by soaking in an ethanol solution of 1,10-phenanthroline therefore implementing a ship-in-the-bottle methodology, post-synthetic Soxhlet extraction allowing to remove unreacted materials.[84] The obtained catalyst was tested in the oxidation of cycloalkanes into the corresponding alcohols and ketones with 30% H_2O_2. The catalyst encapsulated in MIL-100(Al) showed better activity compared to the free copper complex and to the same complex encapsulated in Zeolite-Y. Furthermore, the catalyst was recyclable with no loss of activity over three consecutive runs. A similar approach has been used to incorporate a spin crossover complex in MIL-100(Al) (Fig. 6B).[85] This was performed through impregnation of the MOF with $Fe(NO_3)_3 \cdot 9H_2O$ in a chloroform solution, followed by immersing of the impregnated solid in a solution of sal_2trien ligand to form Fe(sal_2trien)@MIL-100(Al). The obtained composite material was used to sense water molecules at room temperature, and showed reversible colour change upon sorption of this guest molecule.

Pd nanoparticles can also be encapsulated into MIL-100(Al) (Fig. 6C) by immersing the activated MOF into a solution of freshly prepared tetrachloropalladinic acid, followed by reduction of the $PdCl_4^{2-}$ ions into a stream of an Ar/H_2 mixture at 553 K, leading to a Pd@MIL-100(Al) composite with a Pd loading of ~10 wt%.[86] Although the incorporation of Pd nanoparticles through this procedure induced a decrease of the BET surface area of the MOF from 1200 $m^2\ g^{-1}$ to 380 $m^2\ g^{-1}$, the H_2 excess uptake capacity of the MOF at 298 K under a pressure of 4 MPa was increased from 0.19 to 0.35 wt%. This was explained by the

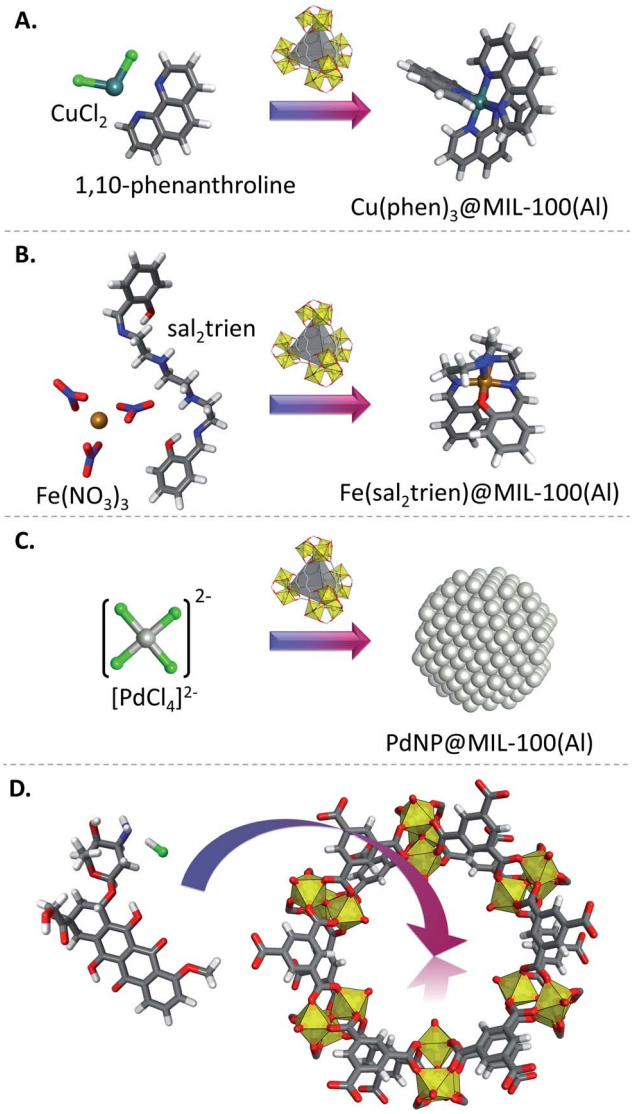

Fig. 6 Encapsulation of (A) a $Cu(phen)_3$ complex, (B) $Fe(sal_2trien)$ complex and (C) Pd nanoparticles in MIL-100(Al) through a ship-in-the-bottle methodology, and (D) encapsulation of deoxyrubicin hydrochloride with an hexagonal window of the large pores of MIL-100(Al) drawn to scale.

formation of palladium hydride, which was evidenced by *in situ* PXRD, as well as by a complementary spillover mechanism. However, the excess uptake capacity at 77 K was higher for the pristine MOF (3.1 wt%) than for the one charged with nanoparticles (1.3 wt%), due to the difference in surface area.

Recently, liquid electrolytes obtained by dissolution of perchlorates of different 1st group (Li^+, Na^+, K^+ and Cs^+) and 3rd period (Na^+, Mg^{2+} and Al^{3+}) cations in propylene carbonate have been incorporated in activated MIL-100(Al) by impregnation, resulting in immobilization of ClO_4^- ions by the CUSs of the MOF.[87] This methodology afforded solid-like electrolytes in which the cations can be transported through the MOF's channels with increasing conductivity from Li^+ to Cs^+, similarly to their liquid counterparts. However, unlike the liquid electrolytes, which show decreasing conductivity ($Na^+ > Mg^{2+} > Al^{3+}$) with increasing charge density, the MOF-based solid-like electrolytes show a maximum of ionic conductivity (1 mS cm^{-1}) and minimum of activation energy (0.2 eV) when Mg^{2+} is used. The solid-like electrolytes obtained by this methodology showed enhanced cycling durability in Na–metal battery cells.

Concerning biomedical applications, MIL-100(Al) xero- and aerogels were studied for the removal of the toxic pollutant microcystin-LR.[57] Aerogels were also used as carriers for the drug deoxyrubicin hydrochloride for anticancer drug delivery purposes (Fig. 6D).[58] Importantly for drug-release applications, it has been shown by *in vitro* experiments that MIL-100(Al) is not cytotoxic but is less stable in cell culture media than its Fe- or Cr-based counterparts.[88]

2.7 Oxides, carbon derivatives and composites made thereof

Due to the presence of organic linkers and aluminium metal centres, various porous materials have been derived from MIL-100(Al). Calcination of MIL-100(Al) at 600 °C for example gives octahedron-shaped γ-Al_2O_3 particles with pores of around 2.4 nm, which are smaller than the ones of the parent MOF.[89] Calcination of MIL-110(Al) gives hexagon rod-shaped particles with larger pores, of around 4.4 nm, showing that the topology of the used MOF dictates the nature of the calcined materials. In a similar way, porous carbons can be derived from the MOF material if the heating is performed under an inert atmosphere. Carbonization of MIL-100(Al) under Ar flow at temperatures between 600 and 1000 °C for example leads to the formation of Al_2O_3 embedded in carbon.[90] Alumina can then be removed from those materials by treatment with HF, yielding hollow octahedral carbon cages. Experiments showed that the carbonization temperature has an important impact on the textural properties of the obtained materials, as heating at 800 °C resulted in a microporous material with the highest BET surface area (1711 m^2 g^{-1}), showing good CO_2 and H_2 adsorption capacities, as well as good removal capacity of methylene blue from aqueous solutions. Alternatively, MIL-100(Al), composites of this MOF with copolymers, or mixtures of this MOF with KOH can be heated under nitrogen at 700 °C and subsequently be washed with HCl to remove aluminium oxides, allowing to obtain microporous carbons with BET surface areas comprised between 253 and 1097 m^2 g^{-1}.[91] The materials obtained in this way present good CO_2 capture and excellent CO_2/N_2 selectivity (45) and good selectivities for CO_2/CH_4 (14.5) and CH_4/N_2 (5.1) gas mixtures. By prior impregnation of the MOFs with *N*-(1-ethyl-3-methylimidazolium dicyanamide) and/or B-containing (1-ethyl-3-methylimidazolium tetracyanoborate) ionic liquids, followed by carbonization and acid washing, (N)- and (BN)-decorated porous carbons can be obtained.[92] Such materials show better CO_2 and H_2 relative uptakes when compared to the non-decorated carbons materials, albeit lower surface areas. Carbonization under nitrogen atmosphere at temperatures between 700 and 900 °C without any acid post-treatment leads to the formation of hierarchical mesoporous graphite oxide/Al_2O_3 materials. Such composites were used for the fabrication of electrodes for the electrochemical determination of caffeic acid in red wine samples.[93]

This journal is © The Royal Society of Chemistry 2021

3. MIL-101(Al)

3.1 Synthesis and thermodynamical stability of NH_2-MIL-101(Al)

The first Al-based MOF with MIL-101 topology and most widely studied MOF of this category, NH_2-MIL-101(Al), was obtained in 2011.[94] It has a reported thermal stability similar to that of MIL-100(Al) (decomposition around 650 K in air according to TGA), and is built from 2-aminoterephthalate linkers. It was first obtained by solvothermal treatment of $AlCl_3 \cdot 6H_2O$ and 2-aminoterephthalic acid in DMF at 403 K for 72 h. The MOF was obtained as a yellow powder, which was washed with acetone and activated in boiling methanol. The use of aluminium nitrate instead of chloride yielded NH_2-MIL-53(Al) and the use of unsubstituted terephthalic acid as linker source resulted in the formation of MIL-53(Al), evidencing the difficulty to selectively obtain MIL-101(Al) compounds. The obtained MOF possessed a BET surface area of 2100 $m^2\ g^{-1}$ and a high thermal stability up to 650 K, quite similar to NH_2-MIL-101(Cr). Similarly to MIL-100(Al), the synthesis time of NH_2-MIL-101(Al) can be significantly shortened (to 20–30 min) by using microwave heating, resulting in the formation of nanocrystals with similar BET surface area (2095 $m^2\ g^{-1}$).[95] The solvothermal synthesis was monitored *in situ* by means of simultaneous SAXS-WAXS measurements.[44,45] Those experiments allowed to evidence the formation of metastable NH_2-MOF-235(Al) in the early stages of the synthesis, this phase being subsequently transformed into NH_2-MIL-101(Al) (Fig. 7, upper part). When water was added to the reaction medium, NH_2-MOF-235(Al) was transformed into NH_2-MIL-53(Al), which seemed to be the thermodynamical product. This was explained by the dissolution of the metastable NH_2-MOF-235(Al) in the presence of water, leading to crystallization of NH_2-MIL-53(Al) from the solubilized precursors (Fig. 7, middle part). The metastable MOF, which is stabilized by DMF, is thus necessary for the formation of NH_2-MIL-101(Al), which likely proceeds through a crystal rearrangement. When the synthesis is performed in pure water as solvent, NH_2-MOF-235(Al) is not formed and MIL-53(Al) is the only species crystallizing from the mixture (Fig. 7, lower part). *In situ* ^{27}Al-, and more importantly ^{1}H-NMR, experiments allowed to determine that the presence of the amine group in the ligand, as well as DMF, allow to stabilize the formation of the $Al_3(\mu_3\text{-}O)$ cluster that composes both NH_2-MOF-235(Al) and NH_2-MIL-100(Al).[46] The experiments also evidenced the formation of a H–Cl–DMF complex species upon dissociation of a water molecule complexed to an Al centre (Fig. 7, inset). The formation of this complex abstracts a proton from the water molecule, forming the hydroxido ligand of the NH_2-MIL-101(Al) SBUs, triggering the topological transformation of the metastable intermediate into the mesoporous MOF. These observations explain why the synthesis only succeeds in the presence of chloride ions and DMF. Those conclusions were corroborated by DFT calculations, which also evidenced an important effect of the solvent and co-solvent used for the synthesis.[96] Similarly to the use of insoluble phosphate for achieving selective synthesis of MIL-100(Al) over MIL-96(Al) and MIL-110(Al), templating agents have shown to be efficient in the selective synthesis of NH_2-MIL-101(Al).[97] Although some studies controvert this,[98] it has been observed by *in situ* SAXS and WAXS analysis that when adding the Keggin polyanion derived from phosphotungstic acid ($H_3PW_{12}O_{40} \cdot H_2O$, or PTA) into the reaction medium, PTA acts as nucleation site for the NH_2-MOF-235(Al) intermediate and stabilizes this species. The final product obtained by this approach however contains encapsulated heteropoly acid (HPA) units. The synthesis of HPA containing NH_2-MIL-101(Al) can also be performed with shorter reaction times of about one hour by applying microwave heating.[99] However, in another study, NH_2-MIL-53(Al) was obtained through this procedure, indicating that even with templating agents, the synthesis of phase-pure NH_2-MIL-101(Al) remains difficult to achieve.[98]

It has also been observed that the concentrations of reactants have an impact on the synthesis outcome. Further improvements of the synthesis include stepwise addition of the aluminium chloride to the reaction mixture,[100,101] or slow addition of this reactant under the form of a solution,[102] which seems efficient to selectively obtain NH_2-MIL-101(Al) with increased surface areas going up to 2970 $m^2\ g^{-1}$.[103] Alternatively, the dissolution of $AlCl_3 \cdot 6H_2O$ in DMF can be performed overnight, before adding the 2-aminoterephthalic acid and heating at 130 °C for 72 h.[104] Those modifications seem to allow obtaining good quality NH_2-MIL-101(Al).

In the literature, many examples dealing with functionalization or applications of NH_2-MIL-101(Al) present PXRD patterns of the compound with either low crystallinity, or the presence of a secondary phase, often ascribed to the more thermodynamically stable NH_2-MIL-53(Al). In some cases, those issues are even overlooked by the authors, which often claim the MOF as being a pure compound despite evident diffraction peaks not explained only by NH_2-MIL-101(Al) phase. Systematic study of the stability of a large panel of well-known and popular MOFs, showed that NH_2-MIL-101(Al) shows quite disappointing results regarding chemical and hydrothermal stability, with loss of crystallinity or transformation to another crystalline phase and loss of surface area upon exposure to air and water (with or without H_2O_2), and even dissolution under acidic conditions ($pH = 0$).[105] Even the copper-based HKUST-1, which is known to possess rather weak stability towards water, performs better than NH_2-MIL-101(Al). This is in sharp contrast with MIL-101(Cr), which was the best performing material in these stability tests, showing a stability even higher than the zirconium-based MOF UiO-66 and its amine-substituted counterpart. Those observations highlight that the nature of the metal(s) composing the SBUs is crucial for the general properties and stability of the framework.

It should be noted that the amine function of NH_2-MIL-101(Al) imparts some interesting properties to this MOF, among which fluorescence. This fluorescence is pH dependent and allows the use of NH_2-MIL-101(Al) as fluorimetric pH sensor for pH values varying between 4.0 and 7.7.[106] This fluorescence is also quenched by ellagic acid, allowing its use as fluorescent probe for detecting and quantifying the presence of this natural phenol compound.[107]

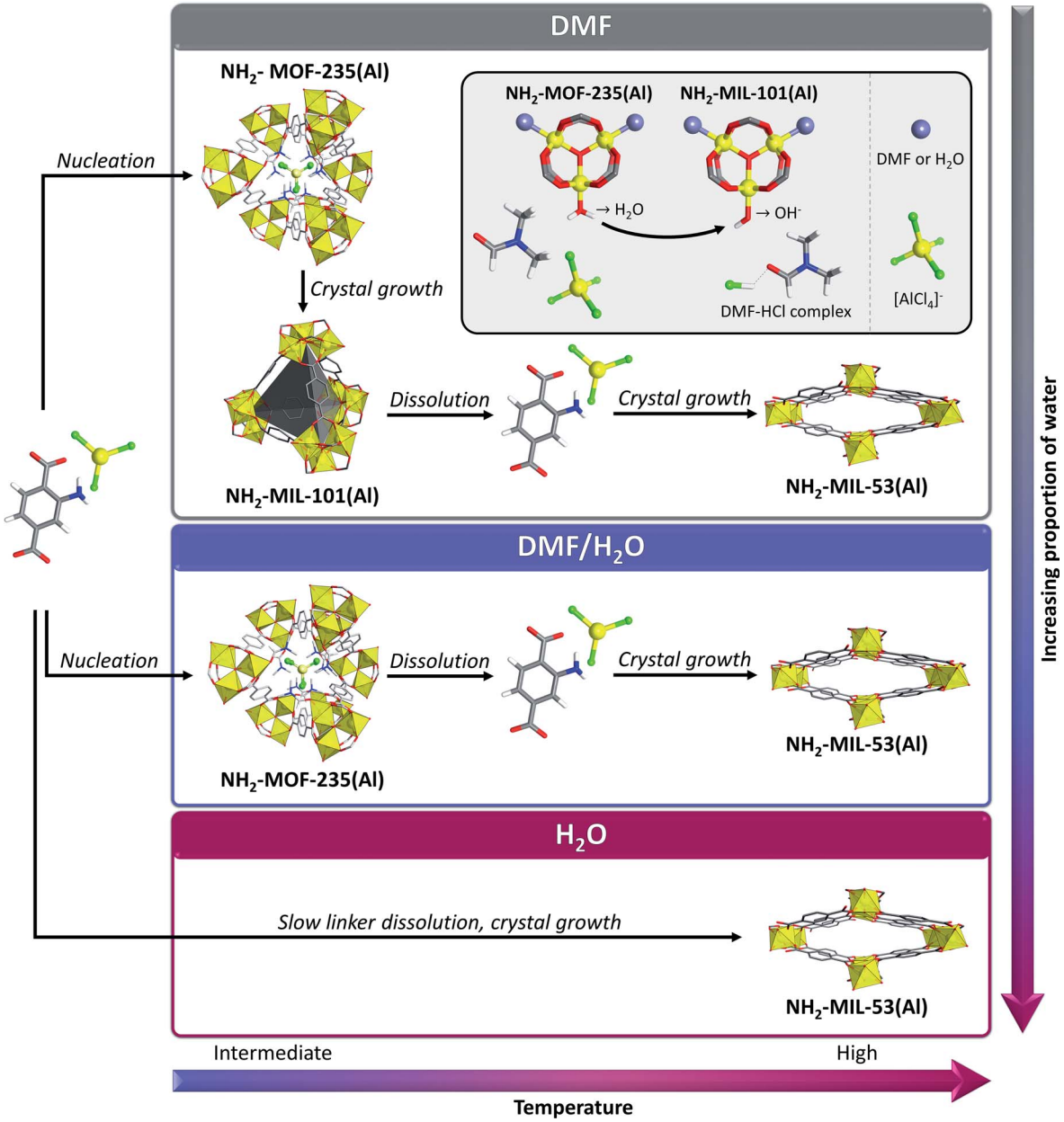

Fig. 7 Formation mechanism of NH_2-MOF-235(Al), NH_2-MIL-101(Al) and NH_2-MIL-53(Al) under solvothermal conditions in DMF/water mixtures starting from 4-aminoterephthalic acid and aluminium chloride, as deduced from *in situ* diffraction experiments. Colour code: yellow = Al, grey = C, red = O. Hydrogen and (disordered) amine functions of the MOFs are omitted for clarity. Adapted from ref. 44 and 46.

MIL-101(Al) MOFs with linkers other than NH_2BDC have also been obtained but they are far less studied. The synthesis and properties of those compounds, including the pristine MIL-101(Al) containing no functionalities on the linkers, are described below.

3.2 Linker functionalities

Although MIL-100(Al) has only been obtained with unsubstituted trimesate linkers, several derivatives of MIL-101(Al) containing modified terephthalate linkers have been obtained. MIL-101(Al) derivatives with $-CH_3$, $-NO_2$, $-OCH_3$, $-C_6H_4$, $-(CH_3)_2$, $-(OCH_3)_2$ and $-F_2$ substituted linkers (Fig. 8B–H.) have been obtained by direct solvothermal reaction of the substituted version of terephthalic acid (H_2BTC-X) with $Al(ClO_4)_3 \cdot 9H_2O$ in *N*,*N*-diethylformamide at 130 °C during 3 to 12 h.[108] Alternatively, the materials could be obtained with reduced reaction times (10 min) using microwave irradiation at 170 °C, however leading to less crystalline products. All those materials show thermal stabilities (260–430 °C), gas sorption and specific BET surface areas (1328–2398 $m^2\ g^{-1}$) which are dependent on the nature of the functionality on the linker. MIL-101(Al) compounds with mixed NH_2BDC^{2-} and pre-synthesized Ph_2PBTC^{2-} linkers (Fig. 8I) have also been obtained through direct solvothermal synthesis in DMF using $AlCl_3 \cdot 6H_2O$ as

 This journal is © The Royal Society of Chemistry 2021

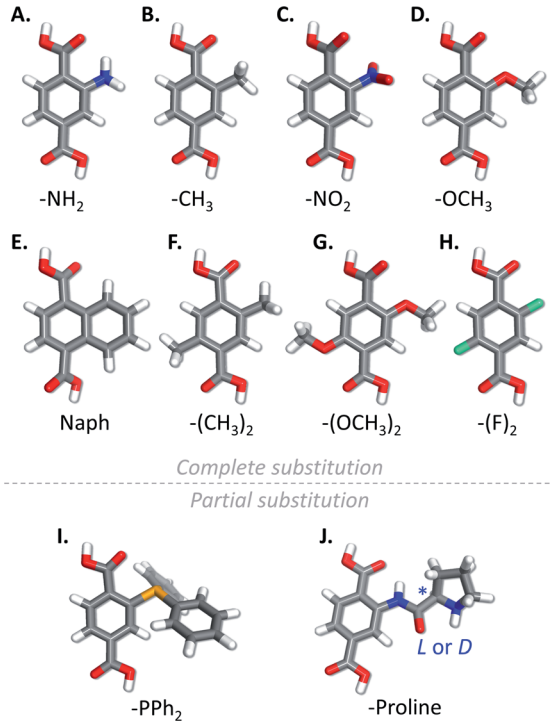

Fig. 8 Linkers from which substituted X-MIL-101(Al) MOFs can be obtained through direct synthesis (in X-MIL-100(Al), X stands for the functionalities on the MOF's linkers), either with complete substitution (A to H) or by partial substitution (I and J).

aluminium source and the acidic form of the linkers, at 110 °C.[102] Boc-L-proline-H_2BDC and boc-D-proline-H_2BDC could also be used to obtain mixed-ligand MIL-101(Al) derivatives through direct synthesis, by using up to 30% mol of the functionalized linker.[109] During the synthesis, the -Boc protecting group was cleaved from the substituted linkers, leading to the incorporation of proline functionalized ligand into the MOFs (Fig. 8J). The used of non-protected proline bearing terephthalic acid for the synthesis resulted in the formation of amorphous compounds. Due to the size of the functionalities, the proportion of incorporated functionalized linkers into the final MOF was less than the engaged one. The obtained proline-decorated frameworks could be used as catalysts for the enantioselective aldol condensation of 4-nitrobenzaldehyde with acetone, the enantioselectivity of the MOF catalysts being the opposite from the one obtained when using proline derivatives in homogeneous conditions.

In one report, the preparation of non-substituted MIL-101(Al) through direct synthesis is described: the MOF was obtained through a procedure similar to the classical pathway for NH_2-MIL-101(Al) by substitution of 2-aminoterephthalic acid by terephthalic acid.[106] This preparation procedure, which yields crystalline MIL-101(Al) in one step is in contradiction with most reports dealing with the synthesis of MIL-101(Al) derivatives, which claim the impossibility of obtaining the unsubstituted MOF though the direct pathway. This could however indicate that very small variations in reaction parameters can drastically affect the outcome of the synthesis. Nevertheless, the BET surface area of the framework obtained in this way is only 712 $m^2\ g^{-1}$, indicating low quality of the obtained MOF, or its incomplete activation. Unsubstituted MIL-101(Al) with a much higher BET surface area of 2445 $m^2\ g^{-1}$ can be obtained through a post-synthetic deamination approach of NH_2-MIL-101(Al).[103] This deamination is performed through reaction of the –NH_2 functionalities of the MOF with *t*-butyl nitrite to form diazonium moieties which can then be removed through heating at 80 °C in methanol (Fig. 9A). Part of the –NH_2 functions of the MOF can be protected prior to deamination by conversion into amides, which are not transformed into diazonium under these conditions (Fig. 9B).

Trimethylsilyl azide can be added to NH_2-MIL-101(Al) reacted with *t*-BuONO in THF, allowing the introduction of azide functions on the linkers of the MOF (Fig. 9C).[110] Those azide functions can be converted back into the fluorescent amines upon reaction with H_2S, providing an efficient way to detect this molecule (*e.g.* in physiological solutions) with a sensitivity increase of three orders of magnitude compared with earlier reported azido-functionalized MOFs.

Other interesting functionalities can be added to NH_2-MIL-101(Al) by taking advantage of the rich amine chemistry. Transformation of those amines into amides is the most straightforward reaction. This can be performed in the absence of solvents, by heating the NH_2-MIL-101(Al) in the presence of acyl chlorides, acid anhydrides or carboxylic acids for short reaction times of 10 min (Fig. 9D).[111] The use of carboxylic acids leads to very low functionalization yields (0 to 4%) but anhydrides and acyl chlorides allow achieving significant functionalization (47 to 92%). This functionalization is most effective when performed with bulky functionalities like *t*-butyl or benzylic moieties, as smaller derivatives such as ethyl groups lead to partial or complete collapse of the MOF structure as revealed by PXRD, likely due to competition between the formed acetic acid and the linker. Peptide functionalities can also be anchored to the MOF through the formation of amide bonds (Fig. 9D).[112] This is performed through microwave or conventional heating of a suspension of NH_2-MIL-101(Al) in DCM in the presence of a coupling agent, a base and a Boc-protected peptide at 80 °C. The –Boc protecting group can then be removed from the attached peptide by short (10 min) microwave irradiation at 150 °C, yielding post-functionalized MOFs with grafting yield between 5 and 60%, depending on the size of the used peptide and the exact reaction conditions. The unaltered chiral functionalities added by this method allow using the compounds in applications such as asymmetric aldol condensations.

By reacting dried NH_2-MIL-101(Al) with suberic acid bis(*N*-hydroxysuccinimide ester) in DMF, a suberate (octanedioate) anchor can be attached to the amine functions of the MOF through the formation of an amide.[113] The second, terminal, succinimide unit of the suberate unit can then be substituted by 4-methylaminopyridine (Fig. 9E). The decorated MOF obtained by this methodology possesses good catalytic activity towards the decomposition of diisopropyl fluorophosphates, a close analogue of sarin gas. Therefore, this material was attached on surfaces by reactive adhesives (polyisobutylene/toluene

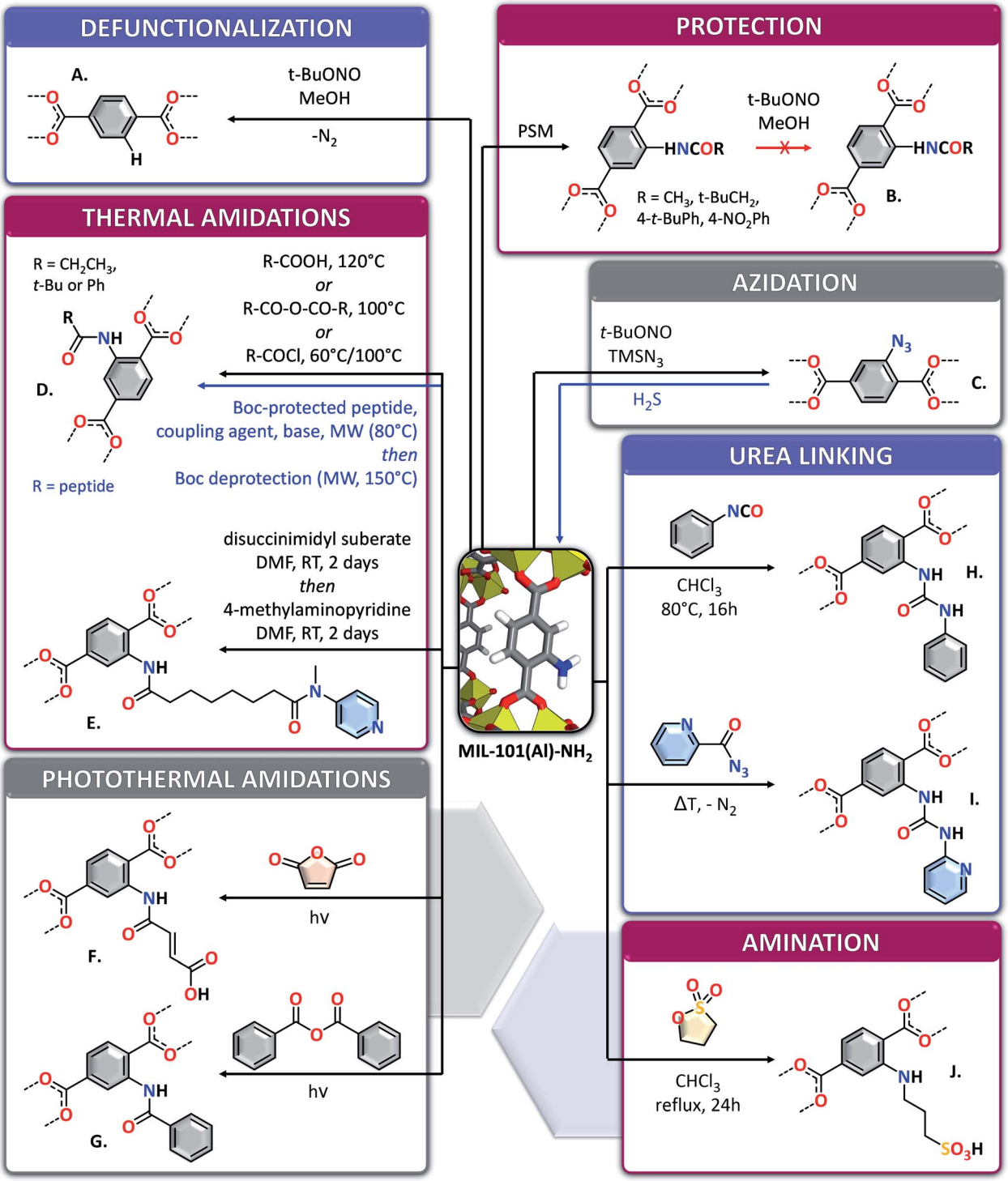

Fig. 9 Different post-functionalization strategies of NH_2-MIL-101(Al) (part 1).

diisocyanate) to endow self-detoxifying properties to the final composites. This approach can be used to cover the surface of elastomeric films for designing self-detoxifying protective gloves, for example. However, one can notice by having a closer look at the PXRD patterns of the functionalized MOF obtained through this methodology that the framework underwent a phase transformation to MIL-53(Al) and partial amorphization. Solid acid anhydrides such as maleic anhydride (Fig. 9F) and benzoic anhydride (Fig. 9G) can also be reacted with the amine functions of NH_2-MIL-101(Al) to form amides without applying external heat.[114] UV-vis irradiation of a solid mixture of the MOF and the anhydride allows the generation of heat through photothermal effect, which could be monitored by infrared imaging and is sufficient to melt the anhydride and

 This journal is © The Royal Society of Chemistry 2021

overcome the activation barrier necessary to enable the formation of the amide. Even if this functionalization strategy does not employ solvents, DMF and acetone are still necessary to activate the MOF.

The formation of urea moieties is another manner to graft new functionalities through the chemistry of the amine groups in NH_2-MIL-101(Al). This can be performed through the reaction of the MOF with phenylisocyanate by heating in chloroform in the presence of methanol (Fig. 9H).[115] The phenyl moieties added through this procedure render the MOF more resistant towards water, both in solution and in vapour phases. Argon, nitrogen and water sorption measurements, together with ^1H–^{27}Al D-HMQC NMR experiments allowed attributing this increased resistance to a shielding mechanism of the aluminium SBUs, rather than pore blocking. Urea-linked functionalities can also be obtained by reaction of 2-pyridyl acyl azide with NH_2-MIL-101(Al) in refluxing dichloromethane, forming reactive 2-pyridyl isocyanate *in situ* in the MOF's pores by a Curtius rearrangement, and allowing the formation of the urea bound species (Fig. 9I) with a 90% functionalization yield.[116] The *in situ* formation of the isocyanate species in this case is important, as 2-pyridyl isocyanate is prone to undergo rapid dimerization, the formed dimer not being able to react with the amines. The pyridyl functionalities incorporated into the MOF by this strategy enable H-bonding with guest molecules.

Sulfonic acid groups could be covalently attached to NH_2-MIL-101(Al) through reaction of the MOF with 1,3-propanesultone in refluxing chloroform, allowing to anchor propyl sulfonic moieties by formation of a secondary amine (Fig. 9J).[117] The Brønsted acidic $–SO_3H$ functions allowed using the MOF as an efficient catalyst for the esterification of acetic acid with *n*-butanol, with activities similar to commercial Amberlyst-15 and Nafion NR50 resins. Salen-like complexes can also be synthesized in NH_2-MIL-101(Al), by reacting the amine functions with salicylaldehyde and cobalt nitrate hexahydrate in ethanol (Fig. 10A).[118] However, in this case only the pyrolyzed compound has been fully characterized and used for applications, whereas FTIR and the colour change of the MOF upon reaction were the only proofs for the formation of the complex inside the MOF. The advantage of the amine functionalities was also taken to graft polymers onto NH_2-MIL-101(Al) nanoparticles. 4-Dimethylaminopyridine, *N*-(3-dimethylaminopropyl)-*N*′-ethylcarbodiimide hydrochloride and 4,4′-azobis(4-cyanovaleric acid) were reacted with the MOF in NMP to form a macro initiator (Fig. 10B).[119] This initiator was subsequently used for the free-radical polymerization of 2-acrylamido-2-methyl-1-propanesulfonic acid (Fig. 10C). The materials obtained in this way display a high density of sulfonic functions, rendering the materials very acidic and promising for applications necessitating proton exchange membranes, such as fuel cells.

3.3 Acid and base catalysis

Due to the amine functionalities of its linker, pristine NH_2-MIL-101(Al) finds some applications in base-promoted catalysis. This MOF has been proven to be an efficient catalyst for the Knoevenagel condensation of benzaldehyde with malononitrile.[100] It has been shown that NH_2-MIL-101(Al) possesses high and similar activity to NH_2-MIL-101(Fe) for this reaction, as well as good recyclability over at least five consecutive runs, with even some improvement after several cycles. The amino functionalized MOF CAU-1 showed less activity due to its smaller pore size. However, in another study it was shown that the more stable NH_2(50%)-MIL-53(Al), composed of a 50/50 ratio of terephthalate and 4-aminoterephthalate linkers, showed better activity for this reaction.[120] Thanks to its Al_3O SBUs, NH_2-MIL-101(Al) also possesses Lewis acidic moieties, similarly to MIL-100(Al) as discussed above. This MOF can thus be used as a bifunctional heterogeneous catalyst with isolated Lewis acid and Brønsted basic sites. This allows to use it for tandem reactions such as Meinwald rearrangement-Knoevenagel condensation[121] or deacetalization-Knoevenagel condensation reactions.[122] For this last reaction, a recent composite material made from NH_2-MIL-101(Al) embedded in an Amberlite IRA900-type resin showed conversions up to 99% for the transformation of benzaldehyde dimethyl acetal into 2-benzylidenemalononitrile after 5 h at 110 °C.[123] This composite material, obtained through a strategy consisting of a combination of ion exchange of the Cl^- ions of the resin with NaOH, followed by a second exchange with 2-aminoterephthalic acid and subsequent solvothermal reaction with aluminium chloride, was easily recoverable by simple decantation.

The amine functionalities also allow important interactions of the linkers of this MOF with carbon dioxide. Therefore, NH_2-MIL-101(Al) has been investigated in the formation of cyclic carbonates from CO_2. The MOF can be used under solvent-free conditions in the presence of *n*-Bu_4NBr as co-catalyst to form cyclic carbonates from styrene oxide.[124] The MOF could be reused over five catalytic cycles with 96% yield, 99% selectivity and a TOF of 23.5 h^{-1}.

3.4 Gas sorption and separation

In relation to the above, NH_2-MIL-101(Al) can be used to efficiently adsorb and separate carbon dioxide in the gas phase. Polysulfone and polyimide polymer matrices were used to construct mixed-matrix membranes with encapsulated NH_2-MIL-101(Al) as filler material.[125] Those membranes showed improved CO_2/CH_4 separation performances in the presence of the MOF filler, especially at higher pressures. However, the use of the smaller-pore NH_2-MIL-53(Al) was proven to be more effective than its NH_2-MIL-101(Al) counterpart. Another study showed that NH_2-MIL-101(Al) is more efficient as filler material in the preparation of sulphur-containing copolyimide mixed matrix membranes for the H_2/CH_4 and CO_2/CH_4 separation than NH_2-MIL-53(Al).[126] However, a closer look at the PXRD patterns of the MOF used for this study reveals that the NH_2-MIL-101(Al) is not pure.

Composite NH_2-MIL-101(Al)/cellulose acetate (CA) hollow fibres materials have been tested as packing material in cryogenic packed bed columns for the separation of carbon dioxide from natural gas with a CO_2 content of 90%.[127] The composite showed better efficiency for this application than commonly

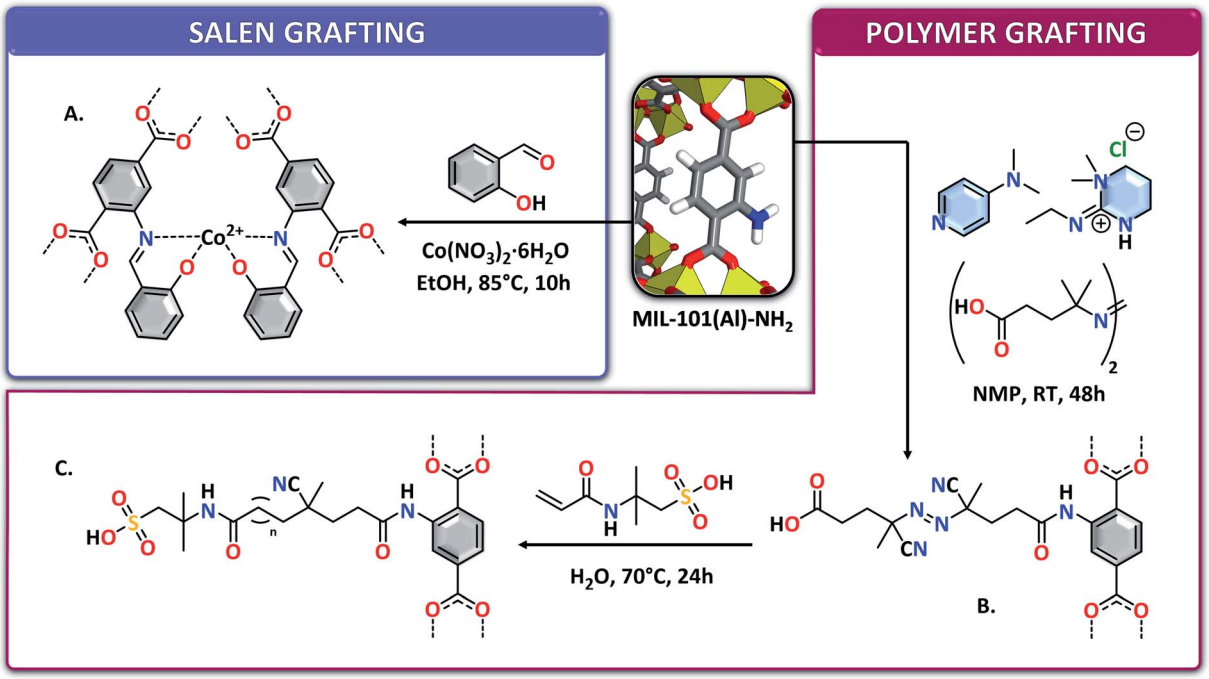

Fig. 10 Different post-functionalization strategies of NH_2-MIL-101(Al) (part 2).

used glass beads, requiring less energy for cooling and allowing higher carbon dioxide capture. The presence of the MOF in the composite was also responsible for enhanced CO_2 capture compared to pristine CA hollow fibres, making this material promising for applications in the cryogenic purification of natural gas. Growing NH_2-MIL-101(Al) on carbon nanotubes (CNTs) by adding carboxylic decorated CNTs to the MOFs reaction mixture, allows to obtain efficient filler materials for preparing mixed matrix membranes for efficient CO_2 separation.[128] Indeed, the decorated nanotubes obtained by this way contain amine functionalities through the presence of NH_2-MIL-101(Al) at their surface, which allow a better dispersion in 4′-(hexafluoroisopropylidene) diphthalic anhydride-durene polymeric membranes than for pristine CNTs. The obtained membrane also demonstrated improved gas permeance and CO_2/CH_4 separation performances than membranes obtained with pristine CNTs.

The hydrogen sorption capacities of NH_2-MIL-101(Al) were also measured experimentally, but the performances were moderate when compared to other MOFs.[129] However, the predicted adsorbate density in this MOF is nearly twice as high as the one of its chromium counterpart, highlighting the importance of aluminium based-MOFs when gravimetric considerations are becoming important.

3.5 Adsorption and separation of dissolved species

In addition to a molecular simulation study which showed that MIL-101(Al) possesses better diffusion and adsorption of terephthalic acid in its structure than its Cr, Fe, V and Mn analogues,[130] several experimental studies were dedicated to the adsorption of molecules from solution or to separations by filtration on materials based on NH_2-MIL-101(Al). It has been shown that the phenol adsorption properties from water of NH_2-MIL-101(Al) is very similar to that of MIL-100(Cr) and MIL-100(Fe).[131] However, the adsorption capacity for *p*-nitrophenol is much higher for NH_2-MIL-101(Al) than for the two other MOFs and even higher than that of very-well performing activated carbons, because of the interaction of the amine functionalities with the adsorbate. NH_2-MIL-101(Al) is also very effective in the adsorption removal of cationic methylene blue (MB) from aqueous solution, however leading to complete loss of crystallinity of the solid and leaching of Al from the MOF, precluding its reusability.[132] Non-functionalized MIL-101(Al) displayed a much lower adsorption, evidencing the role of the amine functions in the adsorption process. The adsorption of anionic methyl orange (MO) by NH_2-MIL-101(Al) is four times lower than of MB but does not affect the integrity of the framework, which can thus be reused for the adsorption of this dye. Another study showed that NH_2-MIL-101(Al) particles with a magnetic Fe_3O_4 core (which allows recuperation by a magnet) have similar adsorption capacities for MO and MB, as well as for malachite green and indigo carmine, and that those materials are reusable for at least five adsorption cycles with no noticeable loss of capacity.[133] The preservation of the material upon adsorption of MB is in contrast with the degradation of bare NH_2-MIL-101(Al) with this dye: the increased stability of the composite material might be explained by the presence of the magnetic core. Inorganic phosphates can also be efficiently removed from aqueous solutions (87.85 $mg_P\ g^{-1}$) through the use of NH_2-MIL-101(Al), which displays higher adsorption kinetics than NH_2-MIL-101(Fe) although this last MOF possesses slightly better affinity and adsorption (94.34 $mg_P\ g^{-1}$) than its aluminium counterpart.[134] NH_2-MIL-101(Al) can be embedded into thermoplastic polyamide-12 by a three-

 This journal is © The Royal Society of Chemistry 2021

dimensional powder printing technique, selective laser sintering, to yield stable mixed-membrane films, which were proven to be efficient in the removal of methylene blue thanks to the presence of the MOF.[135] This provides a more convenient way to handle the MOF material than when it is used as a powder, as the membrane can simply be immersed in, and removed from, the MB solution.

Positively charged filtration membranes showing salt rejection capabilities (in the following order: $MgCl_2$ > $CaCl_2$ > NaCl > Na_2SO_4) were prepared by embedding rod-shaped NH_2-MIL-101(Al) particles in a chitosan polymeric matrix. The obtained membrane displayed rejection capabilities close to the one of a similar membrane made of NH_2-MIL-101(Cr) particles, but showed a two times higher permeability than this second membrane due to the granular shape of the chromium-based MOF.[136] Glycidyl methacrylate monoliths containing NH_2-MIL-101(Al) have been prepared through embedding of the MOF into the polymeric material.[137] The obtained monoliths were tested for the liquid chromatographic separation of polyaromatic hydrocarbons and non-steroidal anti-inflammatory drugs and showed to be more efficient than similar monoliths based on NH_2-MIL-101(Cr) or NH_2-MIL-101(Fe). However, a close look at the reported PXRD patterns reveals important structural differences between the three MIL-101 MOFs used in this study, showing impurities in the Al-MOF and possibly explaining the better performances of the material. Recently, it was shown that NH_2-MIL-101(Al) is able to adsorb up to 457.69 mg g^{-1} of the anti-cancer drug methotrexate from aqueous solutions, demonstrating better performances than MIL-53(Al) and NH_2-MIL-53(Al).[138] The excellent performances of NH_2-MIL-101(Al) for removal of this drug was explained by its larger surface area and pore volume compared to the two other aluminium terephthalate derivatives, as well as to the presence of the polar amino functions and the high positive zeta potential of the MOF.

The presence of three terephthalate linkers on each Al_3O SBU in NH_2-MIL-101(Al) forms cone-like cavities with three exposed aromatic rings. This particular molecular assembly has been shown, by DFT calculation and experimental validation, to have the perfect geometry to accept triethylamine (TEA) molecules through a "lock-and-key" mechanism by interaction of the ethyl functions of the tertiary amine with the aromatic system of the MOF's linkers.[139] The suitability of the size and shape of the MOF with this guest molecule is responsible for particularly high affinity, with $\Delta G = -46.7$ kJ mol^{-1}, which is by far more favourable than the interaction with other guest molecules such as ethylenediamine (-2.20 kJ mol^{-1}). This strong interaction of NH_2-MIL-101(Al) with TEA allows the use of this MOF as an efficient sensor for this molecule, which is a toxic pollutant, in water, as its adsorption is accompanied by a quantitative increase of the MOF's fluorescence.

3.6 Composite materials obtained through encapsulation

Similarly to MIL-100(Al), NH_2-MIL-101(Al) can be used for encapsulation purposes, with even more examples covered in the literature, likely because of the larger pores of this MOF and the presence of the amine functionalities. Palladium nanoparticles can be encapsulated in NH_2-MIL-101(Al) by adjusting the pH to 4 through immersion in aqueous HCl, forming $[NH_3^+$-MIL-101(Al)$]Cl^-$, followed by impregnation with H_2PdCl_4.[140] Reduction of the resulting $[NH_3^+$-MIL-101(Al)$]_2[PdCl_4^{2-}]$ by $NaBH_4$ leads to the formation of Pd@NH_2-MIL-101(Al) (Fig. 11A). The presence of amine functions in the template MOF allows obtaining highly dispersed Pd nanoparticles in the final material, which show good selectivity in the catalytic hydrogenation of biomass-based 5-hydroxymethylfurfural to 2,5-dihydroxymethyl-tetrahydrofuran (DHMTHF). It was shown that the reaction intermediate, 2,5-dihydroxymethylfuran, was preferentially adsorbed into the catalyst, promoting its further hydrogenation to DHMTHF, yielding up to 96% of this product in aqueous conditions at 30 °C. The presence of encapsulated polyoxometalate (POM) species in NH_2-MIL-101(Al), which, as discussed above, can be obtained through direct synthesis in which phosphotungstic acid ($H_3PW_{12}O_{40}$) (Fig. 11B) plays a templating role,[97] can be used to generate well dispersed Pt species.[99] Those are obtained by impregnation of the POM/MOF composite with H_2PtCl_6 in ethanol, generating Pt^{2+} complexes within the substrate. The obtained material can then be reduced by thermal treatment under hydrogen, leading to the presence of both Pt^0 and Pt^{2+} species after treatment at 473 K (Fig. 11C) and to Pt^0 and partially reduced W^{5+} when treating at 573 K (Fig. 11D). This latter solid, containing intermetallic Pt–W species, exhibits the highest catalytic activity towards the oxidation of carbon monoxide in the absence or presence of H_2, with activities similar to noble metal catalysts on reducible supports. The impregnation of NH_2-MIL-101(Al) with phosphotungstic acid (Fig. 11B) was shown to add acidic functionality to the material and to increase its adsorption capacity towards acetaldehyde and butyraldehyde vapours, but not acrolein, although it also decreased the BET surface area of the material.[98] Furthermore, the functionalized materials were shown to be good catalysts for the conversion of acetaldehyde into crotonaldehyde in liquid medium. The incorporation of the zinc-substituted POM $[PW_{11}Zn(H_2O)O_{39}]^{5-}$ through direct synthesis and through post-synthetic impregnation of NH_2-MIL-101(Al) has also been studied (Fig. 11B).[141] Although more POM was loaded into the obtained MOF by direct synthesis than by impregnation, both methods led to the partial transformation of the NH_2-MIL-101(Al) phase to the thermodynamically more stable NH_2-MIL-53(Al). Nevertheless, the obtained materials showed good catalytic activity for oxidative desulfurization of fuels, especially the ones obtained through direct synthesis. A POM-AgCl@NH_2-MIL-101(Al) composite material was also obtained by impregnation of NH_2-MIL-101(Al) (although not phase pure) with $K_6[\alpha$-$AgPW_{11}O_{39}]\cdot 12H_2O$ in a water/methanol solution with an HNO_3-adjusted pH of 4.5.[142] This material contained AgCl particles in the MOF template, as indicated by PXRD. Photoreduction of this composite by irradiation under UV light allowed obtaining a new composite, Ag/POM-AgCl@NH_2-MIL-101(Al), in which part of the silver was reduced to Ag^0 as determined by XPS. A similar composite without POM was also obtained by replacing $K_6[\alpha$-$AgPW_{11}O_{39}]\cdot 12H_2O$ by $AgNO_3$ in the synthetic procedure. When NH_2-MIL-

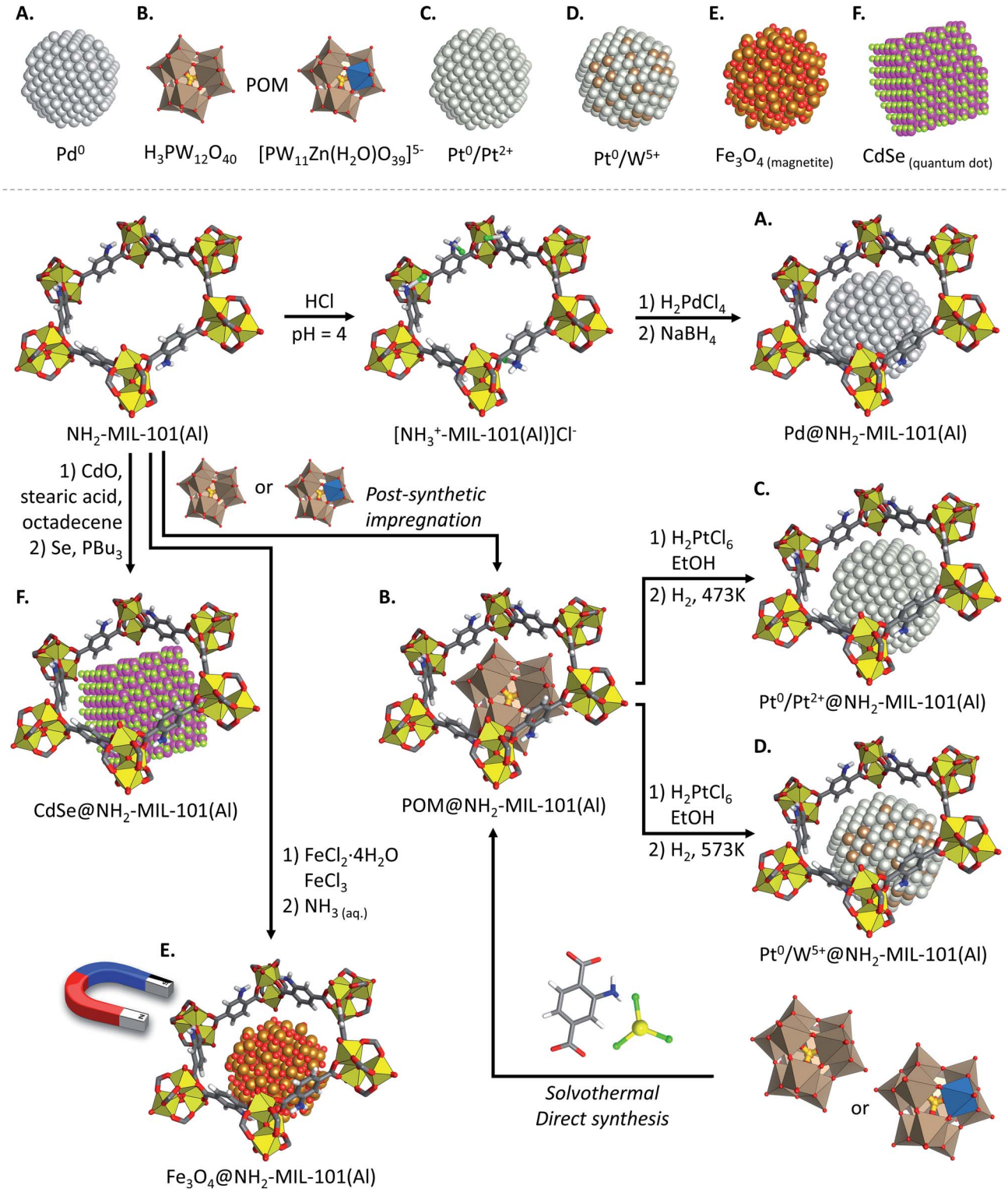

Fig. 11 Nanoparticles (NPs) and polyoxometalates (POMs) that can be encapsulated into NH_2-MIL-101(Al) and synthetic strategies to achieve their encapsulation. (A) Palladium NPs, (B) phosphotungstic acid and zinc substituted POM, (C) platinum NPs, (D) platinum/tungsten bimetallic NPs, (E) magnetic magnetite NPs and (F) CdSe quantum dots.

101(Al) is not used as support for the growth of Ag/AgCl or Ag/POM-AgCl particles, those are obtained as micrometer-sized particles, whereas the use of the MOF allows obtaining nanoparticles, which are very small (3.2 nm) in the case of Ag/POM-AgCl@NH_2-MIL-101(Al). This composite shows better activity towards catalytic reduction of 4-nitrophenol and

 This journal is © The Royal Society of Chemistry 2021

photocatalytic degradation of rhodamine B than its counterpart without POM.

Magnetically recoverable NH_2-MIL-101(Al) can be obtained by embedding Fe_3O_4 nanoparticles into the MOF by reaction with $FeCl_2 \cdot 4H_2O$ and $FeCl_3$ in water, followed by addition of aqueous ammonia to generate Fe_3O_4@NH_2-MIL-101(Al) (Fig. 11E).[106] Alternatively, the Fe_3O_4 nanoparticles can be synthesized *ex situ* and covered with an amine-functionalized silica layer through reaction with tetraethyl orthosilicate and 3-aminopropyltriethylsiloxane, before being added to the MOF precursor solution.[133] Magnetization of NH_2-MIL-101(Al) has also been achieved through mixing Fe_3O_4@SiO_2 magnetic nanoparticles with the MOF under ultrasonication in methanol.[143] This latter composite material was active towards the catalytic formation of cyclic carbonates from carbon dioxide and 1,2-epoxyoctane. The encapsulation of CdSe quantum dots (QDs) in NH_2-MIL-101(Al) has also been performed, through immersion of the MOF into a solution of CdO and stearic acid in octadecene at 503 K, followed by quick injection of a solution of Se and tributylphosphine in the same solvent to initiate the formation of the QDs (Fig. 11F).[144] The use of NH_2-MIL-101(Al) as templating material allowed the growth of densely packed quantum dots with a size of ~2 nm, the amine moieties allowing high loading of metal precursors in the material and passivation of the surface of the obtained luminescent QDs, avoiding the use of protecting agents.

The encapsulation of molecules or complexes into NH_2-MIL-101(Al) has also been studied. The commercially available Jacobsen's salen complex ((*R*,*R*)-(−)-*N*,*N*′-bis(3,5-di-*tert*-butylsalicylidene)-1,2-cyclohexanediaminomanganese(III) chloride) (Fig. 12A) has been encapsulated in NH_2-MIL-101(Al) through a bottle-around-the-ship methodology.[101] The obtained material showed good efficiency for the enantioselective epoxidation of dihydronaphthalene, with enantiomeric excesses similar to the one obtained with the homogeneous Jacobsen complex, along with high TON (~800 h^{-1} for the encapsulated complex *vs.* ~1050 h^{-1} for the homogeneous complex). The catalyst showed good recyclability, maintaining single phase crystallinity of NH_2-MIL-101(Al), over four consecutive runs with no loss of TON or enantioselectivity. The PXRD pattern of the catalyst after reuse however showed decreased peak intensity, which could indicate a loss of crystallinity. The introduction of aluminium isopropoxide (Fig. 12B) in NH_2-MIL-101(Al) has also been investigated by impregnation in toluene.[145] Although PXRD patterns of the MOF before impregnation indicate the presence of some NH_2-MIL-53(Al), the main phase was NH_2-MIL-101(Al). A close look at the PXRD pattern of the MOF after reaction with aluminium isopropoxide reveals that the MOF was transformed into (functionalized) NH_2-MIL-53(Al). The obtained functionalized material however showed good ability to serve as catalyst for the self-condensation of acetaldehyde into ethyl acetate. Ruthenium alkylidene complexes (Hoyveda–Grubbs type complexes) (Fig. 12C) can also be loaded into [NH_3^+-MIL-101(Al)]Cl^- (which can be obtained by treatment of NH_2-MIL-101(Al) with HCl in diethyl ether), by simple adsorption from solution.[104] The MOF retained its crystallinity and phase purity upon adsorption of the ruthenium complexes in DCM and the obtained catalysts showed high activity for olefins metathesis without leaching. The catalyst could even work under continuous flow conditions, demonstrating that homogeneous catalysts can simply and robustly be immobilized in MOFs by simple adsorption. Although the materials showed some deactivation under non-optimized conditions, it was shown in further studies that the amine functionalities of the linkers play no role in this process, neither in the adsorption of the catalyst by the MOF.[108] The incorporation of Hoyveda–Grubbs and similar Zhan type complexes (Fig. 12C and D) has also been attempted by mechanochemical means, by simply milling the complex with the MOF.[146] During this process, conversion of NH_2-MIL-101(Al) to NH_2-MIL-53(Al) having low crystallinity was observed. Noteworthy, dry milling of NH_2-MIL-101(Al) without additives resulted in an amorphization of the MOF. However, the authors excluded a templating effect of the catalyst, as its size does not match with the pore size of NH_2-MIL-53(Al). The obtained NH_2-MIL-53(Al)/Ru catalyst composites showed good activity towards metathesis of olefins, which however shows a significant decrease after several cycles. The authors also demonstrated that such catalysts cannot be incorporated through a bottle-around-the-ship methodology as the ruthenium complex degrades under the solvothermal conditions used for NH_2-MIL-101(Al) synthesis. For incorporation of calix[4]arenes (Fig. 12E), a bottle-around-the-ship methodology however proved to be efficient.[147] In this way, *p*-sulfonatocalix[4]arene (hereafter noted K–SO_3H) and *p*-*tert*-butylthiacalix[4]arene (hereafter Ks–CN), which contain strong –SO_3H and weak –CN functionalities, respectively, were incorporated into NH_2-MIL-101(Al). The acidity of the obtained materials was demonstrated by FTIR spectroscopy by using $CDCl_3$ as probe molecule, which revealed the existence of strong interactions of sulfonic functions in K–SO_3H with the amino functions of the linkers. This was responsible for a lower catalytic activity of the resulting MOF composite compared to the one obtained with Ks–CN, towards the reaction of 1,2-phenylenediamine with ketones to form 1,5-benzodiazepines. When the calix[4]arenes are not encapsulated in the MOF, the opposite reactivity order is observed as the sulfonic functions of K–SO_3H do not interact with amines under these conditions. The Ks–CN@NH_2-MIL-101(Al) composite furthermore was more active than zeolites for the tested reaction.

Complex systems containing two different molecular entities encapsulated in NH_2-MIL-101(Al) can also be obtained. This has been performed through the encapsulation of a molecular complex, $[Cp^*Rh(4,4'\text{-bpydc})]^{2+}$, and a molecular photosensitizer, $[Ru(bpy)_2(4,4'\text{-bpydc})]^{2+}$ (bpydc = bipyridinedicarboxylic acid), by simple impregnation (Fig. 12F).[148] The obtained composite was used as an efficient photocatalyst for the reduction of CO_2 into formate. The study further showed that both metal complexes have different affinity for the MOF template and that they are stabilized into the framework by H-bonding of their –COOH moieties with adsorbed water molecules and the amine functionality of the framework, as well as by π–π interaction between their Cp moiety and the aromatic cycle of the MOF's linker molecules. More recently, the encapsulation of a similar photosystem into NH_2-MIL-101(Al) by

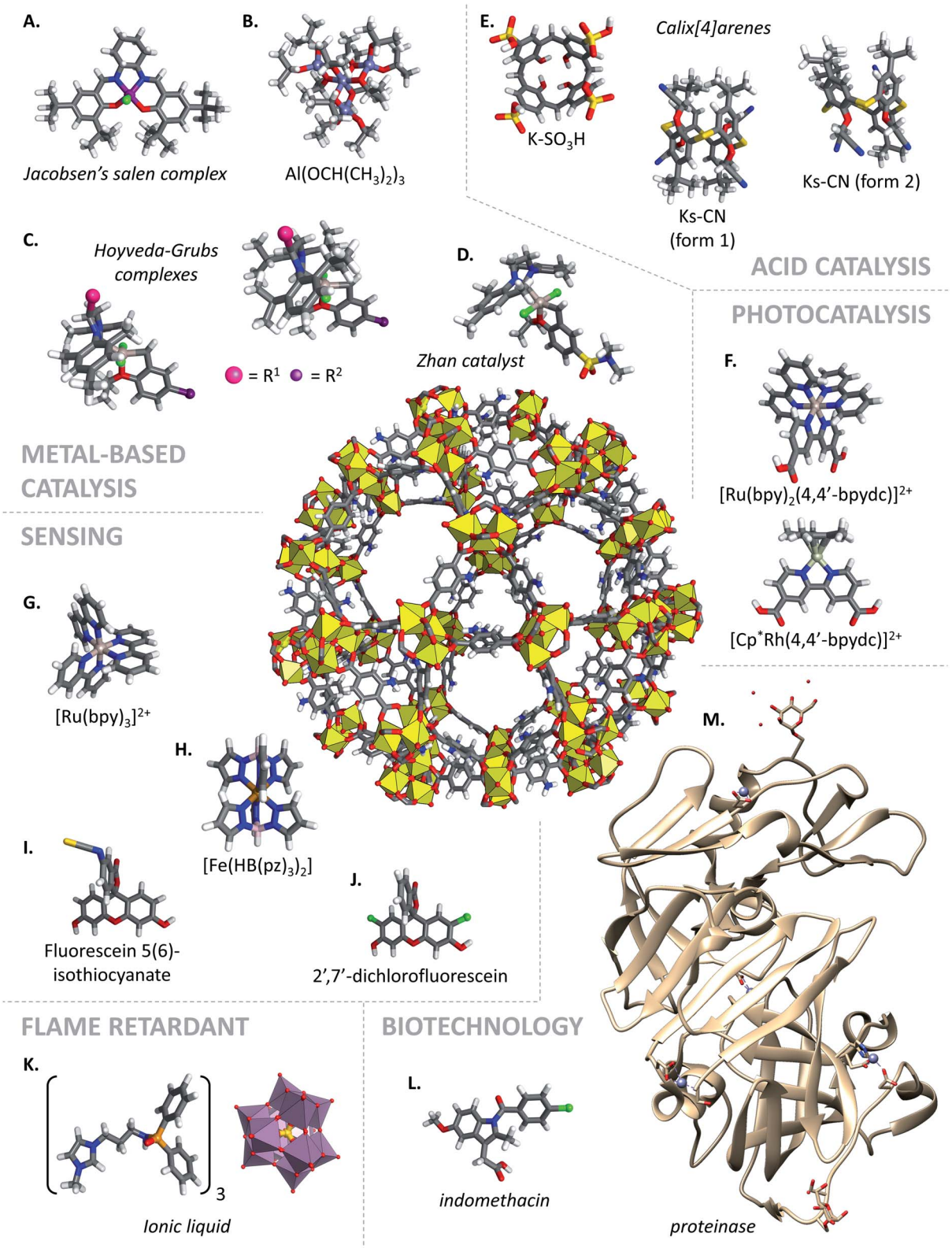

Fig. 12 Molecular species and complexes that have been encapsulated into NH_2-MIL-101(Al) and application domains, along with the large pore of NH_2-MIL-101(Al).

impregnation from acetonitrile solutions has been developed using the benchmark photocatalyst *fac*-ReBr(CO)$_3$(4,4′-dcbpy) (dcbpy = dicarboxy-2,2′-bipyridine) and Ru(bpy)$_2$(5,5′-dcbpy)Cl$_2$ as photosensitizer, allowing to carry out the reduction of CO_2 into CO.[149] This study showed that encapsulation enhanced the stability of the catalyst, the MOF cages acting as nanoreactors.

 This journal is © The Royal Society of Chemistry 2021

The $[Ru(bpy)_3]^{2+}$ complex (Fig. 12G) has also been encapsulated into NH_2-MIL-101(Al) by a bottle-around-the-ship method by incorporating $Ru(bpy)_3Cl_2 \cdot 6H_2O$ into the synthesis mixture of the MOF, which yields a material that can be used for ratiometric fluorescence sensing of water in organic solvents.[127] The obtained $[Ru(bpy)_3]^{2+}$@NH_2-MIL-101(Al) nanoparticles have also subsequently been covered with a polymer layer by reaction with *N*-hydroxy succinimide, *N*-(3-dimethylaminopropyl)-*N*′-ethylcarbodiimidehydrochloride and polyethylenimine (PEI).[150] Gold nanoparticles (AuNP) were then deposited onto the surface of the obtained composite material to yield AuNP/$Ru(bpy)_3^{2+}$@NH_2-MIL-101(Al)@PEI. This luminescent material was used for the design of electrochemiluminescent immunosensors for the detection of procalcitonin (an indicator of septicaemia) in conjunction with another composite material, Ab_2/Cu_xONP/Fe_3O_4@PDA. This second composite is composed of magnetic Fe_3O_4 nanoparticles, covered by a layer of polydopamine (PDA), decorated with Cu_xO nanoparticles and antibodies.

The iron-based spin transition complex bis(hydrotris(pyrazolyl)borato)iron(II) ($[Fe(HB(pz)_3)_2]$) (Fig. 12H) has also been encapsulated into NH_2-MIL-101(Al).[151] This was achieved firstly by a bottle-around-the-ship method, yielding a composite material displaying a colour change from red (low spin state, LS, of the encapsulated complex) to yellow (high spin state, HS) upon heating, over the 300–450 K temperature range. Cooling of the material results in a very slow return to the red-coloured low spin state over a long period, with changes becoming noticeable only after several weeks of storage. Immersion of the compounds into solvents strongly accelerates the HS to LS transition by increasing the local pressure on the complex through the solvents molecules. The same $[Fe(Hb(pz)_3)_2]$@NH_2-MIL-101(Al) compound could also be obtained through gas-phase diffusion of the sublimated complex into the MOF by heating a mixture of both solids in sealed glass tubes under vacuum, followed by washing of the resulting powder with dichloromethane to eliminate any excess of $[Fe(Hb(pz)_3)_2]$.[152]

Fluorescein 5(6)-isothiocyanate (Fig. 12I) has been embedded into NH_2-MIL-101(Al) (presenting some MIL-53 impurity in the PXRD pattern) by soaking the MOF into an ethanolic solution of this fluorescent molecule.[153] The encapsulation of the fluorescein derivative quenched its fluorescence, which could be recovered upon degradation of the MOF by forming stable $[AlF_6]^{3-}$ complex ions by reaction of the Al SBUs with fluoride anions, therefore being able to serve as a sacrificial fluorescent probing material of F^- in solution. A similar strategy to detect fluoride ions, but by chemiluminescence (CL) instead of fluorescence, was adopted by encapsulating 2′,7′-dichlorofluorescein (Fig. 12J) as fluorescent probe.[154] The MOF was incubated in the solution to test, followed by the addition of H_2O_2 and bis(2,4,6-trichlorophenyl)oxalate. In the presence of fluoride anions, the 2′,7′-dichlorofluorescein is released into the solution and triggers a CL reaction with the two aforementioned chemicals, indicating the presence of fluoride anions and allowing their quantification.

Ionic liquids (IL) can be encapsulated in NH_2-MIL-101(Al) to make composite materials. IL@NH_2-MIL-101(Al) with an ionic liquid composed of a diphenylphosphine functionalized imidazole cation and posphomolybdic anion (Fig. 12K) was proven to be an efficient flame retardant for epoxy resins, allowing to reduce the smoke emission of the burning polymer as well as to capture radicals formed during the combustion.[155] The amine functions of the MOF allow increasing compatibility of the composite with the polymer.

As for MIL-101(Fe) and MIL-101(Cr), as well as NH_2-MIL-101(Fe), the encapsulation of the drug indomethacin (Fig. 12L) in NH_2-MIL-101(Al) by adsorption in THF solution has been studied by solid-state NMR.[156] As for its iron and chromium analogues, no interaction of the drug with the framework or amine functionalities was evidenced but instead it has been shown that THF interacts strongly with the metal centres by hydrogen-bonding. The large pores of NH_2-MIL-101(Al) also allow the encapsulation of very large biomolecules such as enzymes. Proteinase from *Aspergillus saitoi* (protease) (Fig. 12M) was introduced into the MOF by incubation in an hexane solution at 60 °C, yielding a protease@NH_2-MIL-101(Al) material.[157] The enzyme, which is much larger than the windows of the MOF, could enter the pores through partial unfolding (translocation), which is favoured by the use of the non-polar solvent and mild reaction temperatures. Encapsulation of the protease within the MOF allowed to stabilize it and take advantage of the catalytic activity of the enzyme under harsh conditions (pH = 1 to 12, temperatures up to 95 °C), in which the free enzyme would degrade. Interestingly, the encapsulated enzyme also displayed higher activity than its free counterpart.

Finally, particles of NH_2-MIL-101(Al) itself can also be encapsulated in another MOF, to create core–shell materials. This has been achieved by synthesizing a layer of the zinc-2-methylimidazolate MOF, ZIF-8, through immersion of the Al-MOF into a methanol solution containing zinc nitrate, 2-methylimidazole and polyvinylpyrrolidone as regulating agent.[158] The core–shell NH_2-MIL-101(Al)@ZIF-8 material was obtained in the form of nanoflowers and could be used for simultaneous removal and detection of Cu^{2+} in water. The removal is performed through the formation of Cu–N bonds thanks to the 2-methylimidazolate linkers of the ZIF-8 shell, whereas the detection is performed through fluorescence quenching of the NH_2-MIL-101(Al) core upon adsorption of Cu^{2+} in the material.

3.7 Oxides, carbon derivatives and composites made thereof

Similarly to MIL-100(Al), NH_2-MIL-101(Al) can been used for obtaining oxide and carbonaceous materials upon calcination or carbonization. The interest of using NH_2-MIL-101(Al) for this purpose lies in the presence of the amine function in the linker, which allows to directly obtain N-doped materials. For example, carbonization of NH_2-MIL-101 at 1073 K under argon atmosphere, followed by treatment with hot hydrochloric acid (333 K) overnight afforded a nitrogen/oxygen dual-doped hierarchical porous hard carbon (NOHPHC) material with a BET surface area of 1030 $m^2\ g^{-1}$, usable as electrode material for potassium-ion batteries.[159] However, the PXRD pattern of the MOF material used in this study showed important peaks of

a secondary crystalline phase, which may affect the properties of the product obtained upon carbonization. Composites of amorphous Al_2O_3 with N-doped porous carbon (NPC) have also been obtained by carbonization of NH_2-MIL-101(Al) under nitrogen atmosphere at 900 °C for 5 h.[160] The obtained Al_2O_3@NPC powder was then embedded in PVDF to make separation membranes for prototypes of Li–S batteries that showed superior performances than pristine separator membranes. Furthermore, the same synthetic procedure was applied by replacing 2-aminoterephthalic acid by therephthalic acid, which gave separation membranes containing Al_2O_3@PC, which showed less optimal performances than the N-doped version. The authors described this as a material obtained from MIL-101(Al) without amine functions, but the PXRD pattern of the material before calcination did not correspond to MIL-101(Al). The preparation of a separation membrane with calcined material from true non-functionalized MIL-101(Al) might give significantly different results. Hierarchically porous N-doped carbon decorated with Pd nanoparticles with catalytic activity in the dehydrogenation of formic acid can also be obtained.[161] This is performed by thermal treatment of the crystallographically pure MOF under argon atmosphere at temperature between 600 °C and 1000 °C, to yield N-doped carbon/Al_2O_3 composites from which the alumina is eliminated through ultrasonication in aqueous KOH. The surface area of the porous carbon materials obtained at this stage showed to be highly dependent on the temperature used for the carbonization process, which was ideal (BET surface area of 1382 $m^2\ g^{-1}$) at 900 °C, lower and higher temperature leading to materials with lower surface areas. Pd nanoparticles were subsequently deposited on the material by impregnation in an aqueous solution containing K_2PdCl_4, followed by reduction with $NaBH_4$ in water. The Pd-loaded composite material obtained from the MOF calcined at 900 °C had a high BET surface area of 1220 $m^2\ g^{-1}$ and demonstrated very high catalytic activity (TOF = 14 400 h^{-1} at 60 °C) and 100% H_2 selectivity towards dehydrogenation of formic acid over 15 cycles. N-Doped carbon composites with CoO nanoparticles have also been obtained through immobilisation of Co^{2+} in the MOF by reaction with salicylaldehyde and cobalt nitrate, followed by pyrolysis under nitrogen atmosphere at temperatures between 700° and 900 °C, and subsequent elimination of aluminium species by NaOH washing.[118] The obtained compounds were used to catalyse the oxygen reduction reaction in a three-electrode cell. N-doped carbon materials which were also used for catalysing the electrochemical O_2 reduction were obtained by carbonizing NH_2-MIL-101(Al) (having a PXRD pattern showing a secondary phase impurity) with or without previous treatment with furfuryl alcohol, under argon atmosphere.[162] By varying the temperature between 550 and 800 °C and by pre-treating or not the MOF material with furfuryl alcohol before carbonization, porous N-doped carbons with different types of nitrogenous functions were obtained. These could be attributed to pyrrolic, pyridinic and quaternary nitrogen atoms in the structure, as identified by XPS. The synthesis and systematic investigation of these materials in the reduction of O_2 allowed determining that the reaction proceeds owing to the quaternary N atoms in N-doped carbons whereas the total nitrogen content has little to no role as the pyridinic and pyrrolic N sites possess negligible activity towards this reaction.

4. Conclusions

Due to the low toxicity, density, wide availability and formation of particularly strong bonds with oxygenated species, MOFs based on aluminium and carboxylate linkers have recently attracted much attention from both the academic and industrial point of view. Among these MOFs, MIL-100(Al) and MIL-101(Al) derivatives are of great interest, mostly because of their large mesoporous cavities and high surface areas. It is thus not surprising that the cavities of both of these MOFs have led to a large and always increasing number of investigations concerning adsorption and encapsulation of many types of chemical species, even as large as small proteins, leading to applications in diverse fields such as catalysis, removal of species from solution, trials of drug delivery, *etc.* Remarkably, encapsulation of otherwise fragile chemical species often leads to their stabilization whereas they are still usable for performing, for example, catalytic (enzymatic) reactions. The catalytic activity of encapsulated species can even be enhanced by the intrinsic catalytic activity of both MOFs due to the presence of the Lewis and Brønsted acidic sites, as well as by the presence of basic sites of amines when using NH_2-MIL-101(Al) as template.

The main drawback of MIL-100(Al) and MIL-101(Al) is their relatively low thermodynamic stability, paired with the co-existence of, respectively, other types of trimesate and (functionalized)terephthalate aluminium-based MOFs, such as MIL-96(Al), MIL-110(Al), MOF-235(Al), MIL-68(Al) and MIL-53(Al). This implies that identification of the crystal structure of the MOF through X-ray diffraction methods should always be performed carefully when using either of those frameworks, at each step of any study, from synthesis through post-functionalization and during applications and re-use, to avoid misidentification. Indeed, any change in synthetic parameters, any interaction with a substrate or any post-functionalization reaction has the potential ability to trigger a structural transformation of the MOF. Such an unnoticed transformation can lead to erroneous assignment of properties (*e.g.* catalytic activity) to the MOF, while actually they arise from products of the framework decomposition. When writing this review, we noticed many misinterpretations of PXRD data, leading to erroneous assignments to either MIL-100, and more often, MIL-101 topologies whereas other frameworks were in fact obtained. Systematic comparison between simulated and experimental PXRD patterns is the best way to avoid such misinterpretations, as both MIL-100 and MIL-101 do not undergo significant structural changes when guests are introduced or removed from the framework, and thus peak positions on powder patterns remain quite constant. It should also be mentioned that only thermogravimetric analysis (TGA) has been used to assess the thermal stability of both MIL-100(Al) and MIL-101(Al) derivatives. However, and especially for the last one, one should be aware that framework degradation (amorphization) can occur at temperatures that are lower than the linker decomposition

 This journal is © The Royal Society of Chemistry 2021

temperature detected by TGA. Therefore, it would be advised to use (variable-temperature) XRD techniques to assess the integrity of the framework in case heating to high temperatures has been carried out.

Noticeably, there are a lot more studies devoted to applications dealing with the MIL-101(Al) topology than with MIL-100(Al), although for this latter one, there are far less reports of structural degradation of the framework during applications. This is partly due to the fact that the first topology is mainly represented by NH_2-MIL-101(Al), and the many post-functionalization possibilities arising from the presence of the amine function on the linker, as well as its intrinsic basicity. The larger size of the cavities of the MOF also partly explain the larger interest in this MOF. However, advantage of the important pore size could also be taken by using pristine, unfunctionalized, MIL-101(Al), which can be obtained from the much cheaper non-functionalized terephthalic acid (H_2BDC). With this in mind, it would be interesting to pursue the development of a controlled direct synthesis method to obtain this MOF from H_2BDC, as only few studies have been devoted to this MOF, which is so far mainly obtained by post-synthetic removal of amine functions from NH_2-MIL-101(Al). The commercial unavailability of functionalized trimesic acid might explain why no MIL-100(Al) derivatives have been obtained with functionalities covalently bound onto the linkers. However, such trimesic acid derivatives were described in recent literature and their incorporation into MIL-100(Al) could lead to interesting compounds, with even better stability compared to their X-MIL-101(Al) derivatives, thanks to the presence of the three carboxylate units of the trimesate linker taking part into the coordinative design of the framework, instead of only two for BDC^{2-} derivatives.

Indeed, for MIL-100(Al) derivatives, there are much less reports of structural degradation upon contact with various solvents or reactive species than for MIL-101(Al) derivatives. However, as noticed previously, checking the framework integrity by means of X-ray diffraction techniques after exposure of those MOFs to conditions that could potentially lead to their structural collapse, is something that is frequently missing. Therefore, it would be useful to have future studies focussing on a systematic evaluation of the stability of both frameworks upon exposure to various solvents, ions and pH conditions to have a clear view on the practical stability window of those MOFs, as was performed in the literature for some other frameworks.[163,164] Ideally, the textural properties should be re-evaluated as well, together with X-ray diffraction patterns of the materials. The detection of defects formation in those MOFs upon contact with various species, through further characterization techniques (bulk and surface spectroscopies) would also be very valuable and is currently missing in the scientific literature.

Remarkably, the large pores of MIL-100(Al) and MIL-101(Al) seem to have attracted most interest of researchers towards their ability to capture relatively large molecules, whereas only a very limited number of studies have been focused on their ability to adsorb gaseous species. We believe, however, that the large surface area and subsequent potential of gas molecules to interact with those MOFs (and their derivatives) might be very interesting for applications in this field. In addition, those MOFs are based on one of the lightest existing metals and could therefore lead to interesting gravimetric sorption capacities, rendering them particularly useful for mobile applications.

Probably because controlled decomposition of MOFs remains a quite expensive way to achieve such compounds, fewer studies have also been devoted to the use of MIL-100(Al) and MIL-101(Al) as well as some of their derivatives as precursors for (functionalized) porous carbons and aluminium oxides. However, the materials obtained by this way demonstrated quite interesting characteristics.

Conflicts of interest

There are no conflicts to declare.

Acknowledgements

The authors acknowledge Dr Koen Robeyns for his help with crystallographic data used for this review and the Fonds de la Recherche Scientifique (F.R.S.-FNRS), Belgium, for funding.

Notes and references

1 E. Barea, C. Montoro and J. A. R. Navarro, *Chem. Soc. Rev.*, 2014, **43**, 5419–5430.
2 J. Li, X. Wang, G. Zhao, C. Chen, Z. Chai, A. Alsaedi, T. Hayat and X. Wang, *Chem. Soc. Rev.*, 2018, **47**, 2322–2356.
3 S. Ramanayaka, M. Vithanage, A. Sarmah, T. An, K. H. Kim and Y. S. Ok, *RSC Adv.*, 2019, **9**, 34359–34376.
4 L. Rani, J. Kaushal, A. L. Srivastav and P. Mahajan, *Environ. Sci. Pollut. Res.*, 2020, **27**(36), 44771–44796.
5 Z. Hu, Y. Wang, B. B. Shah and D. Zhao, *Adv. Sustainable Syst.*, 2019, **3**, 1800080.
6 T. Ghanbari, F. Abnisa and W. M. A. Wan Daud, *Sci. Total Environ.*, 2020, **707**, 135090.
7 N. Gargiulo, A. Peluso and D. Caputo, *Processes*, 2020, **8**, 1–21.
8 H. Wang, Q. L. Zhu, R. Zou and Q. Xu, *Chem*, 2017, **2**, 52–80.
9 R. Zhao, Z. Liang, R. Zou and Q. Xu, *Joule*, 2018, **2**, 2235–2259.
10 C. C. Hou and Q. Xu, *Adv. Energy Mater.*, 2019, **9**, 1801307.
11 X. Zhang, A. Chen, M. Zhong, Z. Zhang, X. Zhang, Z. Zhou and X.-H. Bu, *Metal–Organic Frameworks (MOFs) and MOF-Derived Materials for Energy Storage and Conversion*, Springer, Singapore, 2019, vol. 2.
12 A. Ahmed, S. Seth, J. Purewal, A. G. Wong-Foy, M. Veenstra, A. J. Matzger and D. J. Siegel, *Nat. Commun.*, 2019, **10**, 1568.
13 L. Wang, M. Zheng and Z. Xie, *J. Mater. Chem. B*, 2018, **6**, 707–717.
14 Y. Sun, L. Zheng, Y. Yang, X. Qian, T. Fu, X. Li, Z. Yang, H. Yan, C. Cui and W. Tan, *Nano–Micro Lett.*, 2020, **12**, 103.
15 W.-T. Koo, J.-S. Jang and I.-D. Kim, *Chem*, 2019, **5**, 1938–1963.
16 H. Y. Li, S. N. Zhao, S. Q. Zang and J. Li, *Chem. Soc. Rev.*, 2020, **49**, 6364–6401.

17 W. M. Haynes, *CRC Handbook of Chemistry and Physics*, 97th edn, 2016, pp. 14–17.
18 T. Loiseau, C. Volkringer, M. Haouas, F. Taulelle and G. Férey, *C. R. Chim.*, 2015, **18**, 1350–1369.
19 N. Stock, *Encycl. Inorg. Bioinorg. Chem.*, 2014, 1–16.
20 M. Gaab, N. Trukhan, S. Maurer, R. Gummaraju and U. Müller, *Microporous Mesoporous Mater.*, 2012, **157**, 131–136.
21 L.-H. Schilling, H. Reinsch and N. Stock, *Chem. Met. Fram. Synth. Charact. Appl.*, 2016, 105–135.
22 A. Samokhvalov, *Coord. Chem. Rev.*, 2018, **374**, 236–253.
23 D. Y. Hong, Y. K. Hwang, C. Serre, G. Férey and J. S. Chang, *Adv. Funct. Mater.*, 2009, **19**, 1537–1552.
24 J. L. Schlenker, F. G. Dwyer, E. E. Jenkins, W. J. Rohrbaugh, G. T. Kokotailo and W. M. Meier, *Nature*, 1981, **294**, 340–342.
25 C. Volkringer, D. Popov, T. Loiseau, G. Férey, M. Burghammer, C. Riekel, M. Haouas and F. Taulelle, *Chem. Mater.*, 2009, **21**, 5695–5697.
26 G. Férey, C. Serre, C. Mellot-Draznieks, F. Millange, S. Surblé, J. Dutour and I. Margiolaki, *Angew. Chem., Int. Ed.*, 2004, **43**, 6296–6301.
27 P. Horcajada, S. Surble, C. Serre, D. Hong, Y. Seo, J. Chang and J. Grene, *Chem. Commun.*, 2007, **100**, 2820–2822.
28 T. Loiseau, L. Lecroq, C. Volkringer, J. Marrot, G. Ferey, M. Haouas, F. Taulelle, S. Bourrelly, P. L. Llewellyn and M. Latroche, *J. Am. Chem. Soc.*, 2006, **128**, 10223–10230.
29 C. Volkringer, T. Loiseau, G. Férey, C. M. Morais, F. Taulelle, V. Montouillout and D. Massiot, *Microporous Mesoporous Mater.*, 2007, **105**, 111–117.
30 C. Volkringer and T. Loiseau, *Mater. Res. Bull.*, 2006, **41**, 948–954.
31 P. Long, H. Wu, Q. Zhao, Y. Wang, J. Dong and J. Li, *Microporous Mesoporous Mater.*, 2011, **142**, 489–493.
32 C. Volkringer, D. Popov, T. Loiseau, N. Guillou, G. Ferey, M. Haouas, F. Taulelle, C. Mellot-Draznieks, M. Burghammer and C. Riekel, *Nat. Mater.*, 2007, **6**, 760–764.
33 T. Loiseau, C. Serre, C. Huguenard, G. Fink, F. Taulelle, M. Henry, T. Bataille and G. Férey, *Chem.–Eur. J.*, 2004, **10**, 1373–1382.
34 T. Ahnfeldt, D. Gunzelmann, T. Loiseau, D. Hirsemann, J. Senker, G. Férey and N. Stock, *Inorg. Chem.*, 2009, **48**, 3057–3064.
35 S. Biswas, T. Ahnfeldt and N. Stock, *Inorg. Chem.*, 2011, **50**, 9518–9526.
36 S. Biswas, T. Rémy, S. Couck, D. Denysenko, G. Rampelberg, J. F. M. Denayer, D. Volkmer, C. Detavernier and P. Van Der Voort, *Phys. Chem. Chem. Phys.*, 2013, **15**, 3552–3561.
37 B. Tahmouresilerd, P. J. Larson, D. K. Unruh and A. F. Cozzolino, *Catal. Sci. Technol.*, 2018, **8**, 4349–4357.
38 N. Reimer, B. Gil, B. Marszalek and N. Stock, *CrystEngComm*, 2012, **14**, 4119.
39 D. Himsl, D. Wallacher and M. Hartmann, *Angew. Chem., Int. Ed.*, 2009, **48**, 4639–4642.
40 J. Chen, K. Li, L. Chen, R. Liu, X. Huang and D. Ye, *Green Chem.*, 2014, **16**, 2490–2499.
41 P. Silva, S. M. F. Vilela, J. P. C. Tomé and F. A. Almeida Paz, *Chem. Soc. Rev.*, 2015, **44**, 6774–6803.
42 F. Millange and R. I. Walton, *Isr. J. Chem.*, 2018, **58**, 1019–1035.
43 BASF SE, S. Markus, M. Ulrich and M. Stefan, WO2008129051, 2008.
44 E. Stavitski, M. Goesten, J. Juan-Alcañiz, A. Martinez-Joaristi, P. Serra-Crespo, A. V. Petukhov, J. Gascon and F. Kapteijn, *Angew. Chem., Int. Ed.*, 2011, **50**, 9624–9628.
45 M. G. Goesten, E. Stavitski, J. Juan-Alcañiz, A. Martiñez-Joaristi, A. V. Petukhov, F. Kapteijn and J. Gascon, *Catal. Today*, 2013, **205**, 120–127.
46 M. G. Goesten, P. C. M. M. Magusin, E. A. Pidko, B. Mezari, E. J. M. Hensen, F. Kapteijn and J. Gascon, *Inorg. Chem.*, 2014, **53**, 882–887.
47 M. Haouas, C. Volkringer, T. Loiseau, G. Férey and F. Taulelle, *Chem. Mater.*, 2012, **24**, 2462–2471.
48 N. A. Khan, J. S. Lee, J. Jeon, C. H. Jun and S. H. Jhung, *Microporous Mesoporous Mater.*, 2012, **152**, 235–239.
49 M. Vinu, W. C. Lin, D. S. Raja, J. L. Han and C. H. Lin, *Polymers*, 2017, **9**(10), 498.
50 A. García Márquez, A. Demessence, A. E. Platero-Prats, D. Heurtaux, P. Horcajada, C. Serre, J. S. Chang, G. Férey, V. A. De La Peña-O'Shea, C. Boissière, D. Grosso and C. Sanchez, *Eur. J. Inorg. Chem.*, 2012, **100**, 5165–5174.
51 Y. Fu, K. Li, M. Batmunkh, H. Yu, S. Donne, B. Jia and T. Ma, *ACS Appl. Mater. Interfaces*, 2020, **12**, 44830–44839.
52 B. Barth, M. Mendt, A. Pöppl and M. Hartmann, *Microporous Mesoporous Mater.*, 2015, **216**, 97–110.
53 A. H. Khan, B. Barth, M. Hartmann, J. Haase and M. Bertmer, *J. Phys. Chem. C*, 2018, **122**, 12723–12730.
54 J. Yang, J. Wang, S. Deng and J. Li, *Chem. Commun.*, 2016, **52**, 725–728.
55 B. Seoane, A. Dikhtiarenko, A. Mayoral, C. Tellez, J. Coronas, F. Kapteijn and J. Gascon, *CrystEngComm*, 2015, **17**, 1693–1700.
56 M. Qiu, Q. Guan and W. Li, *Cryst. Growth Des.*, 2016, **16**, 3639–3646.
57 W. Xia, X. Zhang, L. Xu, Y. Wang, J. Lin and R. Zou, *RSC Adv.*, 2013, **3**, 11007–11013.
58 Y. Feng, C. Wang, F. Ke, J. Zang and J. Zhu, *Nanomaterials*, 2018, **8**(6), 446.
59 F. Moreau, J. Marrot, F. Banse, C. Serre and A. Tissot, *J. Mater. Chem. C*, 2020, **8**, 16826–16833.
60 T. Steenhaut, L. Fusaro, K. Robeyns, S. Lacour, X. Li, J. G. Mahy, V. Louppe, N. Grégoire, G. Barozzino-Consiglio, J.-F. Statsyns, C. Aprile, Y. Filinchuk and S. Hermans, submitted, DOI: 10.33774/chemrxiv-2021-hzbc5.
61 A. Martinez Joaristi, J. Juan-Alcañiz, P. Serra-Crespo, F. Kapteijn and J. Gascon, *Cryst. Growth Des.*, 2012, **12**, 3489–3498.
62 M. Haouas, C. Volkringer, T. Loiseau, G. Férey and F. Taulelle, *J. Phys. Chem. C*, 2011, **115**, 17934–17944.
63 F. Pourpoint, A. S. L. Thankamony, C. Volkringer, T. Loiseau, J. Trébosc, F. Aussenac, D. Carnevale,

 This journal is © The Royal Society of Chemistry 2021

G. Bodenhausen, H. Vezin, O. Lafon and J. P. Amoureux, *Chem. Commun.*, 2014, **50**, 933–935.
64 C. Volkringer, H. Leclerc, J. C. Lavalley, T. Loiseau, G. Férey, M. Daturi and A. Vimont, *J. Phys. Chem. C*, 2012, **116**, 5710–5719.
65 A. E. Khudozhitkov, A. V. Toktarev, S. S. Arzumanov, A. A. Gabrienko, D. I. Kolokolov and A. G. Stepanov, *Chem.–Eur. J.*, 2019, **25**, 10808–10812.
66 N. Marshall, W. James, J. Fulmer, S. Crittenden, A. B. Thompson, P. A. Ward and G. T. Rowe, *Inorg. Chem.*, 2019, **58**, 5561–5575.
67 A. A. Taha, L. Huang, S. Ramakrishna and Y. Liu, *J. Water Process Eng.*, 2020, **33**, 101004.
68 A. R. Kim, T. U. Yoon, E. J. Kim, J. W. Yoon, S. Y. Kim, J. W. Yoon, Y. K. Hwang, J. S. Chang and Y. S. Bae, *Chem. Eng. J.*, 2018, **331**, 777–784.
69 M. N. Timofeeva, V. N. Panchenko, A. A. Abel, N. A. Khan, I. Ahmed, A. B. Ayupov, K. P. Volcho and S. H. Jhung, *J. Catal.*, 2014, **311**, 114–120.
70 M. N. Timofeeva, V. N. Panchenko, S. A. Prikhod'ko, A. B. Ayupov, Y. V. Larichev, N. A. Khan and S. H. Jhung, *J. Catal.*, 2017, **354**, 128–137.
71 A. Maity, B. Singh, K. Sharma, S. Paul, P. K. Madhu and V. Polshettiwar, *ACS Mater. Lett.*, 2020, **2**, 699–704.
72 V. N. Panchenko, M. M. Matrosova, J. Jeon, J. W. Jun, M. N. Timofeeva and S. H. Jhung, *J. Catal.*, 2014, **316**, 251–259.
73 M. Mendt, B. Barth, M. Hartmann and A. Pöppl, *J. Chem. Phys.*, 2017, **147**, 224701.
74 M. Chebbi, B. Azambre, C. Volkringer and T. Loiseau, *Microporous Mesoporous Mater.*, 2018, **259**, 244–254.
75 M. D'Amore, B. Civalleri, I. J. Bush, E. Albanese and M. Ferrabone, *J. Phys. Chem. C*, 2019, **123**, 28677–28687.
76 F. Jeremias, A. Khutia, S. K. Henninger and C. Janiak, *J. Mater. Chem.*, 2012, **22**, 10148–10151.
77 T. B. Čelič, M. Mazaj, G. Mali, V. Kaučič and N. Zabukovec Logar, *Proc. 5th Serbian-Croatian-Slovenian Symp. Zeolites*, 2013, pp. 72–75.
78 S. I. Kim, T. U. Yoon, M. B. Kim, S. J. Lee, Y. K. Hwang, J. S. Chang, H. J. Kim, H. N. Lee, U. H. Lee and Y. S. Bae, *Chem. Eng. J.*, 2016, **286**, 467–475.
79 T. Splith, E. Pantatosaki, P. D. Kolokathis, D. Fröhlich, K. Zhang, G. Füldner, C. Chmelik, J. Jiang, S. K. Henninger, F. Stallmach and G. K. Papadopoulos, *J. Phys. Chem. C*, 2017, **121**, 18065–18074.
80 T. Splith and F. Stallmach, *Magn. Reson. Imaging*, 2019, **56**, 52–56.
81 J. W. Jun, M. Tong, B. K. Jung, Z. Hasan, C. Zhong and S. H. Jhung, *Chem.–Eur. J.*, 2015, **21**, 347–354.
82 J. Cai, X. Mao and W. G. Song, *Mater. Chem. Front.*, 2018, **2**, 1389–1396.
83 C. Falaise, C. Volkringer, R. Giovine, B. Prelot, M. Huve and T. Loiseau, *Dalton Trans.*, 2017, **46**, 12010–12014.
84 Y. Chen, B. Fan, N. Lu and R. Li, *Catal. Commun.*, 2015, **64**, 91–95.
85 A. Tissot, X. Kesse, S. Giannopoulou, I. Stenger, L. Binet, E. Rivière and C. Serre, *Chem. Commun.*, 2019, **55**, 194–197.
86 C. Zlotea, R. Campesi, F. Cuevas, E. Leroy, P. Dibandjo, C. Volkringer, T. Lolseau, G. Férey and M. Latroche, *J. Am. Chem. Soc.*, 2010, **132**, 2991–2997.
87 S. Ma, L. Shen, Q. Liu, W. Shi, C. Zhang, F. Liu, J. A. Baucom, D. Zhang, H. Yue, H. Bin Wu and Y. Lu, *ACS Appl. Mater. Interfaces*, 2020, **12**, 43824–43832.
88 R. Grall, T. Hidalgo, J. Delic, A. Garcia-Marquez, S. Chevillard and P. Horcajada, *J. Mater. Chem. B*, 2015, **3**, 8279–8292.
89 D. Liu, F. Dai, X. Li, J. Liang, Y. Liu and C. Liu, *RSC Adv.*, 2015, **5**, 15182–15186.
90 A. Aijaz, J. K. Sun, P. Pachfule, T. Uchida and Q. Xu, *Chem. Commun.*, 2015, **51**, 13945–13948.
91 J. Wang, J. Yang, R. Krishna, T. Yang and S. Deng, *J. Mater. Chem. A*, 2016, **4**, 19095–19106.
92 A. Aijaz, T. Akita, H. Yang and Q. Xu, *Chem. Commun.*, 2014, **50**, 6498–6501.
93 K. Sivasankar, R. Devasenathipathy, S. F. Wang, K. Kohila rani, D. S. Raja and C. H. Lin, *J. Taiwan Inst. Chem. Eng.*, 2018, **84**, 188–195.
94 P. Serra-Crespo, E. V. Ramos-Fernandez, J. Gascon and F. Kapteijn, *Chem. Mater.*, 2011, **23**, 2565–2572.
95 V. I. Isaeva, A. L. Tarasov, L. E. Starannikova, Y. P. Yampol'skii, A. Y. Alent'ev and L. M. Kustov, *Russ. Chem. Bull.*, 2015, **64**, 2791–2795.
96 X. Yang and A. E. Clark, *Inorg. Chem.*, 2014, **53**, 8930–8940.
97 J. Juan-Alcañiz, M. Goesten, A. Martinez-Joaristi, E. Stavitski, A. V. Petukhov, J. Gascon and F. Kapteijn, *Chem. Commun.*, 2011, **47**, 8578–8580.
98 L. Bromberg, X. Su and T. A. Hatton, *ACS Appl. Mater. Interfaces*, 2013, **5**, 5468–5477.
99 E. V. Ramos-Fernandez, C. Pieters, B. Van Der Linden, J. Juan-Alcañiz, P. Serra-Crespo, M. W. G. M. Verhoeven, H. Niemantsverdriet, J. Gascon and F. Kapteijn, *J. Catal.*, 2012, **289**, 42–52.
100 M. Hartmann and M. Fischer, *Microporous Mesoporous Mater.*, 2012, **164**, 38–43.
101 T. Bogaerts, V. Y. D. D. Andy, Y. Y. Liu, F. Lynen, V. Van Speybroeck and V. D. V. Pascal, *Chem. Commun.*, 2013, **49**, 8021–8023.
102 F. L. Morel, M. Ranocchiari and J. A. Van Bokhoven, *Ind. Eng. Chem. Res.*, 2014, **53**, 9120–9127.
103 A. Chołuj, N. I. Nikishkin and M. J. Chmielewski, *Chem. Commun.*, 2017, **53**, 10196–10199.
104 A. Chołuj, A. Zieliński, K. Grela and M. J. Chmielewski, *ACS Catal.*, 2016, **6**, 6343–6349.
105 K. Leus, T. Bogaerts, J. De Decker, H. Depauw, K. Hendrickx, H. Vrielinck, V. Van Speybroeck and P. Van Der Voort, *Microporous Mesoporous Mater.*, 2016, **226**, 110–116.
106 X. Y. Xu and B. Yan, *Dalton Trans.*, 2016, **45**, 7078–7084.
107 C. Lin, Z. Zou, Z. Lei, L. Wang and Y. Song, *Spectrochim. Acta, Part A*, 2020, **242**, 118739.
108 A. Buragohain, P. Van Der Voort and S. Biswas, *Microporous Mesoporous Mater.*, 2015, **215**, 91–97.
109 S. Nießing, C. Czekelius and C. Janiak, *Catal. Commun.*, 2017, **95**, 12–15.

110 A. Legrand, A. Pastushenko, V. Lysenko, A. Geloen, E. A. Quadrelli, J. Canivet and D. Farrusseng, *ChemNanoMat*, 2016, **2**, 866–872.
111 H. Hintz and S. Wuttke, *Chem. Mater.*, 2014, **26**, 6722–6728.
112 J. Bonnefoy, A. Legrand, E. A. Quadrelli, J. Canivet and D. Farrusseng, *J. Am. Chem. Soc.*, 2015, **137**, 9409–9416.
113 L. Bromberg, Y. Klichko, E. P. Chang, S. Speakman, C. M. Straut, E. Wilusz and T. A. Hatton, *ACS Appl. Mater. Interfaces*, 2012, **4**, 4595–4602.
114 J. Espín, L. Garzón-Tovar, G. Boix, I. Imaz and D. Maspoch, *Chem. Commun.*, 2018, **54**, 4184–4187.
115 T. Wittmann, R. Siegel, N. Reimer, W. Milius, N. Stock and J. Senker, *Chem.–Eur. J.*, 2015, **21**, 314–323.
116 T. Wittmann, C. B. L. Tschense, L. Zappe, C. Koschnick, R. Siegel, R. Stäglich, B. V. Lotsch and J. Senker, *J. Mater. Chem. A*, 2019, **7**, 10379–10388.
117 X. Hu, K. Ma, A. Sabbaghi, X. Chen, A. Chatterjee and F. L. Y. Lam, *Mol. Catal.*, 2020, **482**, 110635.
118 L. Chen, Y. Li, N. Xu and G. Zhang, *Carbon*, 2018, **132**, 172–180.
119 H. Mahdavi and L. Ahmadian-Alam, *J. Polym. Res.*, 2015, **22**, 67.
120 F. Martínez, G. Orcajo, D. Briones, P. Leo and G. Calleja, *Microporous Mesoporous Mater.*, 2017, **246**, 43–50.
121 R. Srirambalaji, S. Hong, R. Natarajan, M. Yoon, R. Hota, Y. Kim, Y. H. Ko and K. Kim, *Chem. Commun.*, 2012, **48**, 11650–11652.
122 T. Toyao, M. Fujiwaki, Y. Horiuchi and M. Matsuoka, *RSC Adv.*, 2013, **3**, 21582.
123 Y. Hu, J. Zhang, Z. Wang, H. Huo, Y. Jiang, X. Xu and K. Lin, *ACS Appl. Mater. Interfaces*, 2020, **12**, 36159–36167.
124 S. Senthilkumar, M. S. Maru, R. S. Somani, H. C. Bajaj and S. Neogi, *Dalton Trans.*, 2018, **47**, 418–428.
125 T. Rodenas, M. Van Dalen, P. Serra-Crespo, F. Kapteijn and J. Gascon, *Microporous Mesoporous Mater.*, 2014, **192**, 35–42.
126 B. Seoane, C. Téllez, J. Coronas and C. Staudt, *Sep. Purif. Technol.*, 2013, **111**, 72–81.
127 M. Babar, M. A. Bustam, A. Ali, A. S. Maulud, U. Shafiq, A. M. Shariff and Z. Man, *Cryogenics*, 2019, **101**, 79–88.
128 R. Lin, L. Ge, S. Liu, V. Rudolph and Z. Zhu, *ACS Appl. Mater. Interfaces*, 2015, **7**, 14750–14757.
129 A. Noguera-Díaz, N. Bimbo, L. T. Holyfield, I. Y. Ahmet, V. P. Ting and T. J. Mays, *Colloids Surf., A*, 2016, **496**, 77–85.
130 A. Bigdeli, F. Khorasheh, S. Tourani, A. Khoshgard and H. H. Bidaroni, *J. Inorg. Organomet. Polym. Mater.*, 2020, **30**, 1643–1652.
131 B. Liu, F. Yang, Y. Zou and Y. Peng, *J. Chem. Eng. Data*, 2014, **59**, 1476–1482.
132 E. Haque, V. Lo, A. I. Minett, A. T. Harris and T. L. Church, *J. Mater. Chem. A*, 2014, **2**, 193–203.
133 H. Liu, L. Chen and J. Ding, *RSC Adv.*, 2016, **6**, 48884–48895.
134 R. Liu, L. Chi, X. Wang, Y. Wang, Y. Sui, T. Xie and H. Arandiyan, *Chem. Eng. J.*, 2019, **357**, 159–168.
135 R. Li, S. Yuan, W. Zhang, H. Zheng, W. Zhu, B. Li, M. Zhou, A. Wing-Keung Law and K. Zhou, *ACS Appl. Mater. Interfaces*, 2019, **11**, 40564–40574.
136 X. H. Ma, Z. Yang, Z. K. Yao, Z. L. Xu and C. Y. Tang, *J. Membr. Sci.*, 2017, **525**, 269–276.
137 H. M. Pérez-Cejuela, E. J. Carrasco-Correa, A. Shahat, E. F. Simó-Alfonso and J. M. Herrero-Martínez, *J. Sep. Sci.*, 2019, **42**, 834–842.
138 F. Ahmadijokani, S. Tajahmadi, M. Rezakazemi, A. A. Sehat, H. Molavi, T. M. Aminabhavi and M. Arjmand, *J. Environ. Manage.*, 2021, **277**, 111448.
139 K. Vellingiri, D. W. Boukhvalov, K. H. Kim and L. Philip, *RSC Adv.*, 2019, **9**, 7818–7825.
140 J. Chen, R. Liu, Y. Guo, L. Chen and H. Gao, *ACS Catal.*, 2015, **5**, 722–733.
141 D. Julião, A. C. Gomes, M. Pillinger, R. Valença, J. C. Ribeiro, B. de Castro, I. S. Gonçalves, L. Cunha Silva and S. S. Balula, *Eur. J. Inorg. Chem.*, 2016, **2016**, 5114–5122.
142 J. Yan, W. Z. Zhou, H. Tan, X. J. Feng, Y. H. Wang and Y. G. Li, *CrystEngComm*, 2016, **18**, 8762–8768.
143 M. Nourian, F. Zadehahmadi, R. Kardanpour, S. Tangestaninejad, M. Moghadam, V. Mirkhani, I. Mohammadpoor-Baltork and M. Bahadori, *Catal. Commun.*, 2017, **94**, 42–46.
144 T. Wakaoka, K. Hirai, K. Murayama, Y. Takano, H. Takagi, S. Furukawa and S. Kitagawa, *J. Mater. Chem. C*, 2014, **2**, 7173–7175.
145 L. Bromberg, X. Su and T. A. Hatton, *Chem. Mater.*, 2013, **25**, 1636–1642.
146 J. Spekreijse, L. Öhrström, J. P. M. Sanders, J. H. Bitter and E. L. Scott, *Chem.–Eur. J.*, 2016, **22**, 15437–15443.
147 V. I. Isaeva, M. N. Timofeeva, V. N. Panchenko, I. A. Lukoyanov, V. V. Chernyshev, G. I. Kapustin, N. A. Davshan and L. M. Kustov, *J. Catal.*, 2019, **369**, 60–71.
148 X. Wang, F. M. Wisser, J. Canivet, M. Fontecave and C. Mellot-Draznieks, *ChemSusChem*, 2018, **11**, 3315–3322.
149 P. M. Stanley, C. Thomas, E. Thyrhaug, A. Urstoeger, M. Schuster, J. Hauer, B. Rieger, J. Warnan and R. A. Fischer, *ACS Catal.*, 2021, **11**, 871–882.
150 C. Wang, N. Zhang, D. Wei, R. Feng, D. Fan, L. Hu, Q. Wei and H. Ju, *Biosens. Bioelectron.*, 2019, **142**, 111521.
151 T. Zhao, I. Boldog, V. Spasojevic, A. Rotaru, Y. Garcia and C. Janiak, *J. Mater. Chem. C*, 2016, **4**, 6588–6601.
152 T. Zhao, M. Dong and Y. Zhao, *Appl. Phys. A: Mater. Sci. Proc*, 2019, **125**, 2–7.
153 F. M. Hinterholzinger, B. Rühle, S. Wuttke, K. Karaghiosoff and T. Bein, *Sci. Rep.*, 2013, **3**, 1–7.
154 Y. Sun, X. Xu, Y. Zhao, H. Tan, Y. Li and J. Du, *Talanta*, 2020, **209**, 120582.
155 R. Huang, X. Guo, S. Ma, J. Xie, J. Xu and J. Ma, *Polymers*, 2020, **12**, 1–16.
156 T. Čendak, E. Žunkovič, T. U. Godec, M. Mazaj, N. Z. Logar and G. Mali, *J. Phys. Chem. C*, 2014, **118**, 6140–6150.
157 J. Navarro-Sánchez, N. Almora-Barrios, B. Lerma-Berlanga, J. J. Ruiz-Pernía, V. A. Lorenz-Fonfria, I. Tuñón and C. Martí-Gastaldo, *Chem. Sci.*, 2019, **10**, 4082–4088.
158 L. Zhang, J. Wang, X. Ren, W. Zhang, T. Zhang, X. Liu, T. Du, T. Li and J. Wang, *J. Mater. Chem. A*, 2018, **6**, 21029–21038.

 This journal is © The Royal Society of Chemistry 2021

159 J. Yang, Z. Ju, Y. Jiang, Z. Xing, B. Xi, J. Feng and S. Xiong, *Adv. Mater.*, 2018, **30**, 1–11.
160 S. Deng, Y. Yan, L. Wei, T. Li, X. Su, X. Yang, Z. Li and M. Wu, *ACS Appl. Energy Mater.*, 2019, **2**, 1266–1273.
161 Q. Wang, N. Tsumori, M. Kitta and Q. Xu, *ACS Catal.*, 2018, **8**, 12041–12045.
162 E. Haque, A. Zavabeti, N. Uddin, Y. Wang, M. A. Rahim, N. Syed, K. Xu, A. Jannat, F. Haque, B. Y. Zhang, M. A. Shoaib, S. Shamsuddin, M. Nurunnabi, A. I. Minett, J. Z. Ou and A. T. Harris, *Chem. Mater.*, 2020, **32**, 1384–1392.
163 M. E. A. Safy, M. Amin, R. R. Haikal, B. Elshazly, J. Wang, Y. Wang, C. Wöll and M. H. Alkordi, *Chem.–Eur. J.*, 2020, **26**, 7109–7117.
164 B. Liu, K. Vikrant, K. H. Kim, V. Kumar and S. K. Kailasa, *Environ. Sci.: Nano*, 2020, **7**, 1319–1347.